Master's thesis

NTNU
Norwegian University of Science and Technology
Faculty of Engineering
Department of Energy and Process Engineering

Sigurd Skoglund

High Temperature Heat Pumps Using Zeotropic Refrigerant in Integrated Energy Systems.

Master's thesis in Energy and Environmental Engineering
Supervisor: Trygve Magne Eikevik
Co-supervisor: Ganesan Palanichamy
June 2022

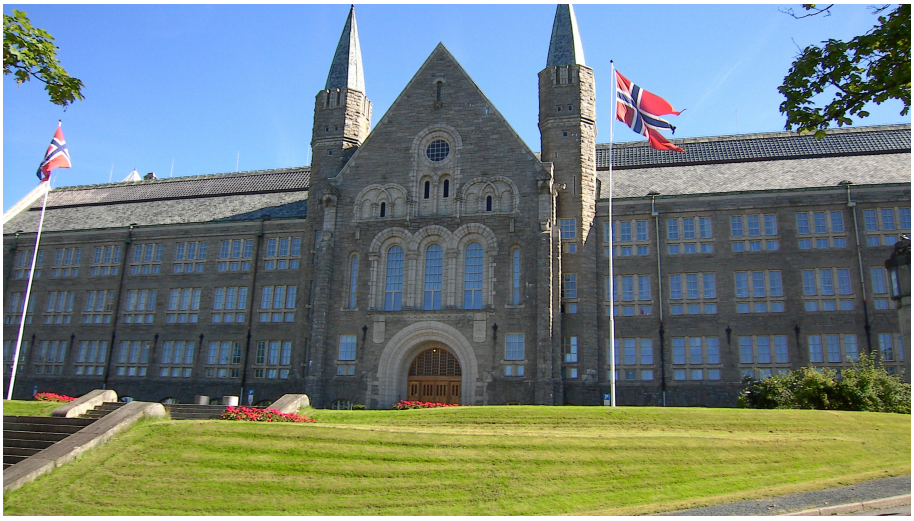

NTNU
Kunnskap for en bedre verden

Sigurd Skoglund

High Temperature Heat Pumps Using Zeotropic Refrigerant in Integrated Energy Systems.

Master's thesis in Energy and Environmental Engineering
Supervisor: Trygve Magne Eikevik
Co-supervisor: Ganesan Palanichamy
June 2022

Norwegian University of Science and Technology
Faculty of Engineering
Department of Energy and Process Engineering

NTNU
Norwegian University of
Science and Technology

Norwegian University of Science and Technology

Faculty of Engineering
Department of Energy and Process Engineering

NTNU

MASTER'S THESIS

for

Sigurd Skoglund

Spring 2022

High Temperature Heat Pump in Integrated Energy Systems

Background and objective

Combined cooling, heating and power generation system meets the need of low-carbon neighborhood to fully absorb renewable energy. A development of load peak-shaving technology of renewable energy based on solar energy with thermal energy storage (TES), as well as the new solar-thermal converting devices, with high-temperature heat pump and compact energy storage system (PCM). At the scenario of 100% clean energy, to achieve a high proportion of renewable energy acceptance by energy supply system in large public buildings or small-scale neighborhoods. In such systems it is necessary to develop high temperature electric heat pump using green or natural working fluid, which the hot side outlet temperature can reach to 100^{o}C, the temperature rise can exceed 50^{o}C, and the COP of the heating system can exceed 3.6. Evaluate different system solutions and alternative natural working fluids to be able to fulfill the requirement. The project is linked to the ChiNoZEN project at NTNU and SINTEF in close cooperation with Chinese universities, especially Shanghai Jiao Tong University.

The following tasks are to be considered:

1. Literature review of high temperature heat pumps in integrated systems
2. Furter development of the software for optimization for transient operations
3. Optimize refrigerant and configuration to suit large temperature glide
4. Investigate influence on seasonal coefficient of performance related to the design point of system
5. Calculate the potential of high temperature heat pump in the integrated system
6. Make a draft scientific paper of the main results in the thesis
7. Make proposal for further work

Contents

List of Figures

List of Tables

List of abbreviations

CO_2	Carbon dioxide
COP	Coefficient of performance
GWP	Global warming potential
$HTHP$	High Temperature Heat Pump
HX	Heat Exchanger
IHX	Internal Heat Exchanger
K	Kelvin
kg	kilogram
$LMTD$	Logarithmic Mean Temperature Difference
$NTNU$	Norwegian University of Science and Technology
ODP	Ozone Depletion Potential
PV	Photovoltaics
PVT	Photovoltaic-thermal
LS	Low stage
HS	High stage
kPa	Kilo pascal
GJ	Giga joule
NG	Natural gas
PCM	Phase change material
$BTES$	Borehole thermal energy storage
kW	kilowatt
GHG	Greenhouse gas
kWh	Kilowatt hour
TES	Thermal energy storage
BHE	Borehole heat exchanger
DHW	Domestic hot water

Abstract

An integrated energy system that consists of a high temperature heat pump (HTHP),a borehole thermal energy storage (BTES), a photovoltaic/thermal (PVT) system, a battery, and a thermal energy storage (TES) was modelled in Matlab and investigated. The high temperature heat pump was modelled as a cascade heat pump using propane in the low stage (LS), and a zeotropic mixture in the high stage (HS). The zeotropic mixture consist of 5 % Carbon Dioxide (CO_2) and 95 % Butane.

The simulation is based on weather data from Oslo, Norway in 2005. The energy system was supposed to be simulated every hour throughout the year. Due to some internal problems in the software and some malfunctions in the code, the simulation was quite restricted. The entire energy system was simulated only for a short period in June, while other components were simulated over the entire year. At every iteration, heat demand, electric power and heat available was calculated which decided the operation of the heat pump.

The heat pump operated with a coefficient of performance (COP) of 3, when the evaporation temperature was 34 $°C$ and the condensing pressure was 1825 kPa, resulting in a temperature rise of 76 $°C$. The heat pump was dimensioned to produce 250 kW, and the maximum capacity of the TES and battery was 1000 kWh, and 250 kWh, respectively. The temperature glide of the refrigerant in the condenser was 29 $°C$, which was a quite good match to the water which was heated 38 $°C$.

The results showed that during a short period in June, the heat demand was covered for in almost the entire period, but in a few hours the energy system was operating insufficiently. During this period, the heat demand from the district heating system was low and the solar irradiance was high, compared to the other seasons. This shows that during the other seasons the energy system will be operating insufficiently for longer periods, more frequently.

The main shortcoming of the energy system is the low heat source temperatures during the year. The PVT system is unable to produce enough heat for most parts of the year, resulting in low evaporation temperatures. Additionally, the performance of the heat pump is quite poor. An optimization of the temperatures and pressure levels in the two stages should be conducted in order to increase performance. Based on the results presented in the thesis, a larger area of the PVT panels should be used in order to increase the heat source temperature. A second heat source could be used, as well. The heat capacity of the heat pump could also be larger, and also the maximum heat capacity of the TES.

Sammendrag

Et integrert energisystem som består av en høytemperatur varmepumpe, termisk energilager i bakken, et solcelle paneler, et batteri og et termisk energilager ble modellert i Matlab og undersøkt. Høytemperatur varmepumpen ble modellert som en kaskadevarmepumpe som bruker propan i den nedre delen, og en zeotropisk blanding i den øvre delen. Den zeotropiske blandingen består av 5 % karbondioksid (CO_2) og 95 % butan.

Simuleringen er basert på værdata fra Oslo i 2005. Energisystemet skulle simuleres hver time hele året. På grunn av noen interne problemer i programvaren og noen feil i koden, var simuleringen ganske begrenset. Hele energisystemet ble simulert kun i en kort periode i juni, mens andre komponenter ble simulert for hele året. Ved hver iterasjon ble det beregnet varmebehov, elektrisk energi og tilgjengelig varme som avgjorde driften av varmepumpen.

Varmepumpen drev med en COP på 3, når fordampningstemperaturen var 34 $°C$ og kondenseringstrykket var 1825 kPa, noe som resulterte i en temperaturøkning på 76 ^{circ}C. Varmepumpen var dimensjonert for å produsere 250 kW, og maksimal kapasitet på varmelageret og batteriet var henholdsvis 1000 kWh og 250 kWh. Temperaturglidingen til kjølemediet i kondensatoren var 29 $°C$, som passet ganske bra til vannet som ble varmet opp 38 $°C$.

Resultatene viste at varmebehovet i løpet av en kort periode i juni ble dekket i nesten hele perioden, men i løpet av få timer fungerte energisystemet utilstrekkelig. I denne perioden var varmebehovet fra fjernvarmeanlegget lavt og solinnstrålingen høy, sammenlignet med de andre årstidene. Dette viser at i de andre årstidene vil energisystemet fungere utilstrekkelig i lengre perioder, oftere.

Hovedmangelen ved energisystemet er de lave varmekildetemperaturene i løpet av året. Solcelle panelene er ikke i stand til å produsere nok varme de fleste delene av året, noe som resulterer i lave fordampningstemperaturer. I tillegg er ytelsen til varmepumpen ganske dårlig. En optimalisering av temperaturer og trykknivåer i de to trinnene bør utføres for å øke ytelsen. Basert på resultatene presentert i oppgaven, bør et større areal av solcelle panelene brukes for å øke varmekildetemperaturen. En annen varmekilde kan også brukes. Varmekapasiteten til varmepumpen kan også være større, og også den maksimale varmekapasiteten til den termiske lagringen

Preface

I would like to thank my supervisor Professor Trygve Magne Eikevik from NTNU and my co-supervisor postdoctoral Fellow Ganesan Palanichamy for their guidance with this project. Their help with this thesis have been crucial for the ending result. They have been easy to communicate with over Mail, and I feel more than welcome to visit their office. I always felt like I could ask them anything regarding the thesis work, and they would guide me and give tips to solve different issues.

After five years as a master student at NTNU, I would like to thank all of the friends that I have made throughout these wonderful five years. I will thank my family for always rooting for me and supporting me during my time as a student. These five years have been truly wonderful, and I have learned a lot academically and also personally.

1 Introduction

1.1 Motivation

The climate crisis regarding the release of green house gases (GHG) has been a highly debated topic throughout the last decades, and is also one of the most engaging topics today. According to *Greenhouse Gas Emissions from Energy Data Explorer – Analysis - IEA* (n.d.), energy accounts for $\frac{3}{4}$ of all GHG emissions globally. When fossil fuels are burned GHGs such as CO_2 forms as a byproduct of the process and accumulates in the atmosphere. In 2019, fossil fuels accounted for 80 % of the total energy supply globally, resulting in large amounts of GHG emissions.

During the last year, the overall share of heating equipment used globally has been dominated by burners using coal, oil and natural gas, which are all fossil fuels. However, in 2020 the share of sales of these equipment fell under 50 %. This shows that the market is transitioning from a fossil fuel-dominated market to a market consisting of more energy efficient and green solutions. Additionally sales of heat pumps and renewable heating equipment made up 20 % of overall installations in 2020. *Heating – Analysis - IEA* (n.d.)

In the Net Zero Emissions by 2050 scenario, the share of heat pumps and renewables-based heating exceeds 80 % of sales in 2030. *Heating – Analysis - IEA* (n.d.) This shows that new heat pump technology is a large potentials in the market in the coming years. Especially heat pump technologies utilizing green energy, such as the one discussed in this thesis will dominate the market more and more according to the existing trends. According to the IEA, efficiency improvements, fuel-shifting and power sector decolonisation would reduce building's heating related emissions by over 50 % by 2030. *Heating – Analysis - IEA* (n.d.)

Today, heat pumps only meet 7 % of global heating needs in buildings, while this share need to be 20 % by 2030. As mentioned the trend is promising, with a 7 % increase in heat pump installation in Europe from 2019 to 2020. The total installed solar thermal heat capacity have also expanded a lot during the past years. In 2010, the total installed solar thermal heat capacity was 230 GW, while ten years later, in 2020, the amount has been more than doubled to 500 GW. *Heating – Analysis - IEA* (n.d.)

1.2 Literature review

1.2.1 High Temperature Heat Pump

Chamoun et al. (2014) performed an experimental and a numerical investigation of a HTHP for industrial heat recovery where water was the chosen refrigerant. The temperature range that was investigated was 130-140 °C. A dynamic model was developed in Modelica and the heat pump was also designed and built on a laboratory test bench. The performance results of the numerical and experimental model was compared and analyzed. The heat pump consist of an evaporator, flash tank, compressor, expansion valve, accumulator, condenser and circulation pumps. In addition to the heat pump, two hydraulic circuits are modeled; one high temperature loop and one low temperature loop.

The flash evaporation system is implemented to avoid overly large heat exchangers. Water vapor have a high specifc volume at 80-90 °C which causes large heat exchangers to allow phase changes. In addition to the flash evaporation system, a purging valve is implemented on top of the accumulator following the condenser to evacuate air. The paper presents some challenges regarding water as the working fluid and state that compressor technology is the main obstacle. To obtain high compression, corresponding to a temperature rise of 40 K, high volumetric flow capacity, and a high isentropic efficiency, a new twin screw compressor has been launched. The compressor offers a compression ratio corresponding to a temperature lift of 40-50 K, and an estimated adiabatic and volumetric efficiency of 57% and 82%, respectively.

The evolution of evaporation and condensation pressures and temperatures obtained from the numerical simulation showed good agreement with the results obtained experimentally. However, some differences were discovered. Differences in evaporation temperature and pressure were caused by the assumption of homogeneous fluid in the simulation, which was not the case in the experiment. The heat pump developed, showed good performance. The waste heat was recovered and increased from 85 to 95 °C, while attaining a condensation temperature of 145 °C and a COP of 5.

Zou et al. (2020) investigated the performance of a air source high temperature cascade heat pump with vapor injection. The vapor injection is introduced due to the high temperature elevation of 120 °C. The system contains a vapor injected R241fa cycle for the high stage, and a R410A cycle for low stage. The paper focused on temperature matching between the heat exchange branches to get optimal heating performance.

The vapor injection technique can increase the mass flowrate in the cycle and therefore reduce the compressor discharge temperature. This will lead to an improvement of the system efficiency. A Genetic Algorithm was used to obtain the optimal intermediate temperature and the vapor injection temperature. The heating COP was calculated to vary from 1.16 to 1.58 for ambient temperature varying from -10 °C to 20 °C. The system also showed better performance for injection pressures lower than the geometric average of the evaporating and condensating pressure in the high stage.

He et al. (2015) did an experimental study on the performance of a vapor injection HTHP. The HTHP is providing hot water at 88 °C. The system consist of standard HTHP supplied with an economizer vapor injection. The economizer acts like an IHX at the condenser outlet. A small part of the liquid refrigerant is sent from the economizer to a manual expansion valve. Then it returns to the economizer to cool the main refrigerant stream coming from the condenser, and turns to superheated vapor.

The effect of the injection pressure were investigated by increasing the injection pressure from 0.82 MPa to 0.98 MPa. It was found that the heating capacity and power consumption increased with 7% and 8%, respectively. Thus, the system COP did not show any significant change. The condensation pressure were also investigated and was varied from 1.19 MPa to 1.51 MPa. In that case, the heating capacity decreased with 12% and the power consumption increased with 21.6%

resulting in a decrease of 27% in system COP. The major benefit of the economizer vapor injection was found out to be the protection of the electric expansion valve (EEV). This was done by providing 16 °C subcooling of the refrigerant, ensuring that the EEV could operate reliably.

Yu et al. (2014) investigated the experimental performance of a single-stage HTHP with a near-azeotropic refrigerant mixture called BY-4. The refrigerant is binary, environmentally friendly, non-toxic and non-flammable. It was found from the experiment that the evaporator water temperature affected the performance of the HP more than the condenser water temperature. When the difference between the condenser outlet water temperature and the evaporator inlet water temperature was less than 30 °C, the COP was higher than 3.5 always. The investigation was done in a range of 77.53 °C to 111.8 °C discharge temperature.

Mota-Babiloni et al. (2018) performed an optimization analysis of a cascade HTHP using IHX in both stages. Different low GWP refrigerants were used in both stages. The effect of the IHXs are investigated by analyzing the COP, the intermediate temperature and discharge temperature in both stages. When the effectiveness of both IHXs are increased, total COP is also increased. A higher HS IHX effectiveness increased the HS discharge temperature but decreased the LS discharge temperature. The LS IHX effectiveness had low impact on the HS discharge temperature but increased the LS discharge temperature. It was concluded that the LS IHX effectiveness should obtain the highest possible value, if the limiting HS or LS discharge temperatures were not reached.

An optimization algorithm was implemented and aimed to maximize the total COP by varying the intermediate temperature, which in turn affect the effectiveness of the IHXs. The optimization algorithm suggested to have an LS IHX effectiveness of unity while the HS IHX effectiveness was dependent on the chosen refrigerants. From the volumetric flow rate and COP point of view butane and isobutane was the most suitable LS refrigerants. On the other hand, from the volumetric flow rate and heating capacity point of view, propane and HFO-1234yf was the most suitable refrigerants. The maximum highest COP was obtained to be 3.15, while using pentane/butane.

1.2.2 Mixed refrigerant HP

Zuev et al. (2020) investigated the efficiency of an autocascade and a cascade heat pump in a cold climate. The autocascade heat pump is based on the zeotropic property of mixed refrigerants. The chosen working fluid was a mixture of R32/R134a/R365mfc for the autocascade process, and R410a and R134a were chosen for the cascade system. The use of the separator in the system causes different refrigerant compositions in different parts of the installation. The results showed that below an ambient temperature of -15 °C, the autocascade performed better in terms of COP. The lower the ambient temperature, the better was the autocascade system.

Fernández-Moreno et al. (2022) did an evaluation of optimal refrigerant mixture in HTHPs. The evaluation was based on multiple parameters, such as COP, VHC, flammability, GWP and perfect glide matching. The refrigerants was also required to have a critical temperature above 150 °C in order to be evaluated. This is why, fluids like propane and carbon dioxide was not part of the

evaluation. Thirteen candidates were evaluated, including the natural refrigerants R-601, R-600, R-600a and R-717. The evaluation is done using a modeled single-stage heat pump with an internal heat exchanger. The heat sink outlet temperature was set to 150 °C and the heat source inlet temperature was set to 70 °C, with a 10 °C temperature glide in each heat exchanger.

The paper doesn't consider GWP a critical parameter, and considers multiple non-zero GWP mixtures. On the other hand, flammability is presented as a critical parameter. The refrigerants with the highest COP have in common that all contain R-601. The mixture that obtain the highest COP is R-601/1234ze(Z). It is a low GWP, flammable, and zeotropic mixture. At the same time, it is expected to experience low pressure drops due to the viscosity and high heat of vaporization. In the A2L saftey class R-1233zd(E)/R-601/R-152a and R-1233zd(E)/R-601/R-161 shows the best performance in therms of COP. In the heat pump system considered in this paper, only natural refrigerants were considered. Also, the investigated condensing temperatures were considerably lower than those used in Fernández-Moreno et al. (2022).

Guo et al. (2019) performed a performance analysis of a high temperature heat pump, using a zeotropic mixture. The zeoptropic mixtures obtain large temperature glide in the subcritical region and the performance is compared with cycles operating in the supercritical region using CO_2, which is more common. A genetic algorithm is used, just as Fernández-Moreno et al. (2022) did, in order to optimize the cycle. The system that is investigated is heating water from 15 °C to 99 °C, using air as the heat source, and consider five different binary mixtures as working fluids. The system is using a recuperative heat exchanger to avoid two-phase refrigerant to enter the compressor. The mixtures that have been chosen consist of one high-boiling point component and one low-boiling point component in order to obtain such a large temperature glide in the heat exchanger.

The paper concluded that the operating pressure and the zeotropic mixtures greatly affected the system performance. n-hexane/propene with a optimal mole fraction of 0.14/0.86 and discharge/suction pressure of 1409.5/704.0 kPa, performed the best with a COP of 5.063. There is also small exergy losses due to a good temperature match between n-hexane/propene and the heat sink. The mixture is outperforming CO_2 heat pump cycles as well, with low operating pressures below 2000 kPa.

Dai et al. (2015) performed a thermodynamic assessment of low GWP CO_2 blends for a heat pump water heater. The system was a basic system consisting of an evaporator, a condenser/gas cooler, a compressor and an expansion valve. The effects that discharge pressure, component ratio, hot water outlet temperature and cold water inlet temperature had on the COP was investigated and analyzed. The maximum COP was obtained at a corresponding optimal discharge pressure, allowing two pinch points to form in the gas cooler/condenser. All of the mixtures experienced subcritical operation at lower X_{CO_2} except CO_2/R41. The temperature match in the evaporator is affecting the system performance greatly, and a good temperature match will reduce irreversibility. From the ten different blends, the CO_2/R41 and CO_2/R32 were the recommended blends.

Sarkar & Bhattacharyya (2009) did an assessment of blends of CO_2 with R600 and R600a as working fluids in medium and high temperature heat pump applications. The mixture mass fraction that is investigated is 50/50. The system consisted of an evaporator, condenser, compressor and expansion valve as well as an internal heat exchanger. The COP and VHC were compared between the two blends and the pure fluids R600, R600a and R744, and the effects of the IHX and the mixture composition were also analyzed.

The results showed that the pure fluids outperformed the blends when the secondary fluid was kept at constant temperature. The blends obtained lower COP, higher VHC, higher pressure ratio and higher throttling losses compared to the hydrocarbons. While for a secondary fluid inlet temperature of 30 °C, and an outlet temperature of 73 °C and 100 °C the blends were better on all the above mentioned parameters. For the 73 °C case, R600a/R744 performed the best while for the 100 °C, R600/R744 performed best. At the 73 °C case, the R600a/R744 mixture performs better than R600/R744 for higher mass fractions of R744, while the optimal mixture mass fraction for both blends was about 0.3 R744.

1.2.3 Solar assisted heat pump

Yao et al. (2020) conducted a performance analysis of a residential heating system consisting of a borehole heat exchanger, a PVT system and a heat pump. The borehole heat exchanger consist of two coaxial pipes, which form the inner and outer pipes. The borehole is 2500m deep, and circulating water will flow and extract heat from the rock-soil. The solar assisted heat pump consists of PVT collector/evaporator, compressor, condenser and expansion valve. The PVT collector/evaporator produce heat to water and electricity to the compressor and pumps.

The heating system operates in three operating modes. When there is lack of solar radiation, only the borehole heat exchanger (BHE) is operating, and all of the water from the users is going through the BHE. In the event of a surplus of solar heat, the BHE is turned off and only the solar assisted PVT heat pump is operating. In the third operating mode, the heating from the BHE and HP alone is unable to meet the demand. Therefore the water from the users are first heated to an intermediate temperature level by the BHE, and the heated to a high-temperature level by the PVT solar assisted heat pump.

The effects of the system operating conditions and physical structure parameters on system performance were numerically investigated. The results showed that with increasing water mass flow in the BHE, the outlet water temperature and BHE system COP decrease, while heat extract capacity and flow resistance increase. Larger outer pipe diameters were found to be better for the circulating water to extract heat from the rock-soil and reduce flow resistance and pump power. The area of the PV/T module was 1000 m^2, the solar irradiation was 600 W/m^2 and the solar fraction was 67.5 %. The system produced in total 542 kW of heating power, where 57 % were produced by solar energy, 33 % were produced by BHE, and the remaining 10 % were produced by the heat pump, and the heating COP could reach 7.4.

Lazzarin & Noro (2020) conducted an analysis of the optimum energy and economic sizing of a dual source heat pump system based on performance. A building in northern Italy will be equipped with a heat pump system using PVT collectors and the ground as sources. The system provides space heating and cooling, ventilation and domestic hot water, and the maximum cooling and heating load the system provides is 21.6 kW and 44.6 kW, respectively. The system consists of four main loops: PVT - source tank - Ground loop, domestic hot water (DHW) loop, Heat Pump - Chiller loop, and Heating - DHW loop. The proposed system provides recharging of the ground by cooling the PVT collectors and thus maintain a high electric efficiency during the summer. Furthermore, multiple storage tanks are used to decouple the heat sources from the heat pump. This is done due to simultaneous heating and cooling loads, when the heat pump operates as a chiller with heat recovery.

Five different alternatives of numbers of boreholes and PVT collector areas were analyzed. The length of the ground probe can be reduced by increasing the PVT collector area, due to larger contribution from solar energy in terms of both thermal and electrical energy. Due to this, the alternative with the largest PVT collector area of 60 m^2 were chosen and three ground probes of 100 m each.

A energy and economic comparison were made with a traditional system consisting of a natural gas fired condensing boiler and an air cooled chiller. On an annual basis, the traditional plant primary energy consumption was 198.5 GJ, while the proposed plant obtained a surplus of 116.7 GJ. In terms of economic performance, the proposed plant saves in annually 7468 € in electricity production from the PVT collectors. The plant also has a 983 € annually expense for electricity from the grid, and 3015 € for investment cost, thus obtaining a net saving of 3470 €. The traditional system has an expense of 705 € for electricity and 4481 € for natural gas (NG) consumption.

Qu et al. (2016) performed an experimental study on the operating characteristics of a PVT integrated dual-source heat pump water heating system. The system used water in the PVT system and air source to produce domestic hot water, and simultaneously cool the cooling water for the PVT collectors to increase the electric efficiency. An experimental setup of the system was established in Shanghai to evaluate its performance. Different air source, inlet water and hot water temperatures were considered and investigated.

At a hot water temperature of 50 °C and a inlet water temperature of evaporator of 10 °C, 20 °C, and 30 °C, the COP obtained was 2.63, 3.6, and 5.05, respectively, showing that system could work efficiently. When the inlet water temperature was higher than 20 °C, the water-water mode obtained higher COP, while in the temperature range of 10-20 °C, the system COP in the two working modes were almost the same. In 270 days, the PVT panel temperature was over 25 °, meaning that the system can work efficiently in water-water mode in 80.7% of the time during the year. The water-water mode can work more efficiently than the air-water mode during winter as well. The air-water mode work on cloudy and rainy days, which provides continuous hot water, efficiently.

Banister & Collins (2015) developed and analyzed the performance of a dual tank solar-assisted heat pump system. The system consist of a PVT system, a float tank, a heat pump, a heat exchanger and a DHW tank. The float tank makes it possible to collect additional solar energy compared to a solar DHW system. The float tank 'float' in temperature, and the efficinecy of the PVT collectors are increased when the temperature is lower in the float tank than in the DHW tank, due to decreases thermal losses. A TRNSYS model was made to design the different control strategies and to determine the optimal working mode.

There are five different working modes considered in the paper. The first priority of working modes is the Solar-DHW mode, which collects solar energy and send it to the DHW tank through a heat exchanger. The next mode, after using mode 1, is to use the heat pump to increase the temperature and energy output. When the solar energy availability is low, the energy stored in the float tank is sent to the DHW tank through a heat exchanger. The fourth mode uses the heat pump to boost the energy output from the float tank. The fifth mode is used when there is no demand, and the solar energy is sent to the float tank for later use.

The simulation was performed on an annual basis for a residential household, with a daily water demand of 300 L. The system is compared to a system using only the first mode of operation. The higher the PVT collector area is, the higher are the energy savings. For a 10 m^2 area, the solar assisted heat pump (SAHP) system obtained 12% higher energy savings compared to the base case. However, the cost of an additional storage tank and a heat pump is high in context of a single-residential. In terms of load scale, the system would be more suited for a multi-residential or district heating application.

1.3 Research question

In this thesis, a Matlab model was created to simulate an integrated energy system. The model was updated from the project work, done prior to this thesis. The energy system consist of a photovoltaic/thermal system, a battery, a borehole thermal energy storage, a high temperature heat pump and a thermal energy storage. The overall system produce 100 % green energy. The PVT system produce electric energy to run the compressors, and produce heat to increase the heat source temperature. The BTES is applied to store excess heat produced by the PVT system, while the battery is applied to store excess electric energy. The heat pump produce high temperature heat to a district heating system, and the TES will store any excess heat produced by the heat pump. The simulation is based on weather data from Oslo, Norway in 2005. The main objective of this thesis is to investigate the performance of the heat pump in coherence with the other constituents of the energy system.

1.4 Scope

This report strictly considers the technical aspects of the aforementioned energy system. In essence, economical aspects are neglected in this thesis. The high temperature heat pump is the main focus of the thesis, and therefore the heat pump model contains the fewest simplifications of the energy system.

2 Theory

2.1 zeotropic mixtures

Zeotropic mixtures, also referred to as nonazeotropic mixtures in the literature, are mixtures of pure refrigerants which have different boiling points. Radermacher & Hwang (2005) Thus, during an evaporation, the most volatile component will boil off first, and the least volatile component will boil off last. The opposite happens during condensation; the least volatile component will condense first, and the most volatile component will condense last. This induces the mixture to evaporate or condensate over a temperature range along the heat transfer surface, at a given fixed pressure. *5.7 Azeotropic/Zeotropic refrigerants - SWEP* (n.d.).

In a temperature-mass fraction diagram a zeotropic mixture is recognized by the difference in mass fraction of vapor and liquid phases in a phase equilibrium. This is seen in figure 1a. During a condensation at a given mass fraction, the temperature will drop from a point on the dew line, and move vertically down to the boiling line, hence experiencing a temperature drop. During an evaporation on the other hand, the mixture will rise in temperature. Generally, the temperature glide increase with increasing difference between the boiling points of the components in the mixture. An example of an azeotropic mixture is shown in figure 1b. Here, it is shown that for a given mass fraction, the mass fraction of vapor and liquid phase are identical. This is referred to as the azeotropic point in the figure. At this point, the mixture condensates or evaporates at constant temperature and pressure. Hence, the mixture behave exactly as a pure refrigerant. For all other mass fractions, the mixture experiencing zeotropic behaviour. Radermacher & Hwang (2005)

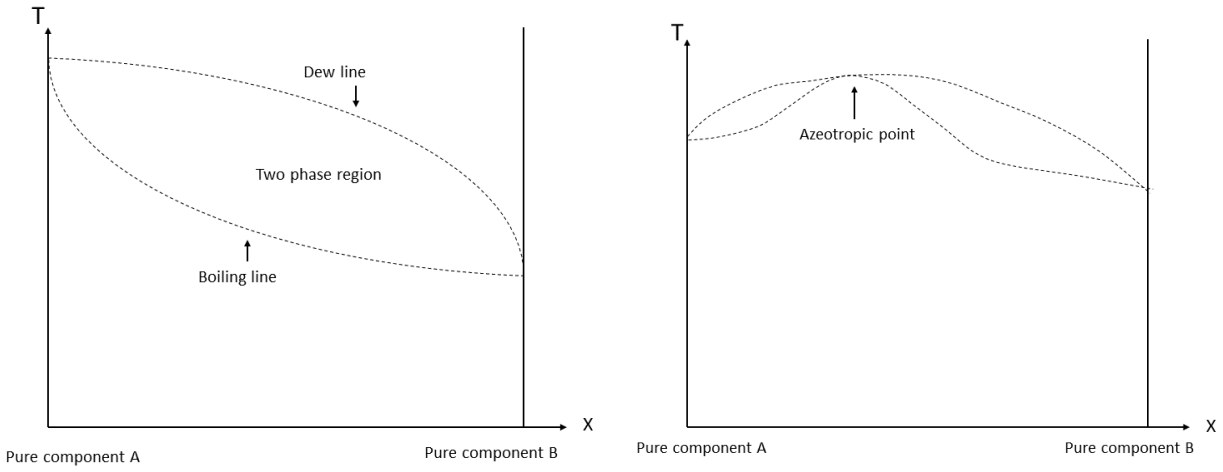

(a) *zeotropic* **(b)** *azeotropic*

Figure 1: *T-x*

The main advantage for a zeotropic mixture is to match the temperature glide in the condensation or evaporation with the temperature glide of the secondary fluid that is to be heated or cooled. If the secondary fluid change in temperature, the Carnot cycle is not preferred as a reference cycle.

The Carnot cycle operates at a constant temperature during condensation and will therefore cause a poor temperature match between the refrigerant and the secondary fluid. When there is large temperature differences between the refrigerant and the secondary fluid, the heat exchange demand more energy than the theoretical minimum.

In figure 2, four different processes are drawn in an temperature-entropy diagram. In case A and C, there is a relatively small temperature change in the secondary fluid, making the Carnot cycle the better reference cycle, compared to the Lorentzen cycle in case C. The surplus heat demand, which emerge as the irreversible losses are the areas marked with a "+" in the figure. In the case of a large temperature rise in the secondary fluid, which is illustrated in case B and D, the Lorentzen cycle is clearly achieving smaller losses than the Carnot cycle. The smaller the temperature difference between the refrigerant and the secondary fluid, the smaller the losses. Hence, using a zeotropic mixture when a secondary fluid is experiencing large temperature glides are favorable, in order to achieve less irreversible losses. Eikevik (n.d.)

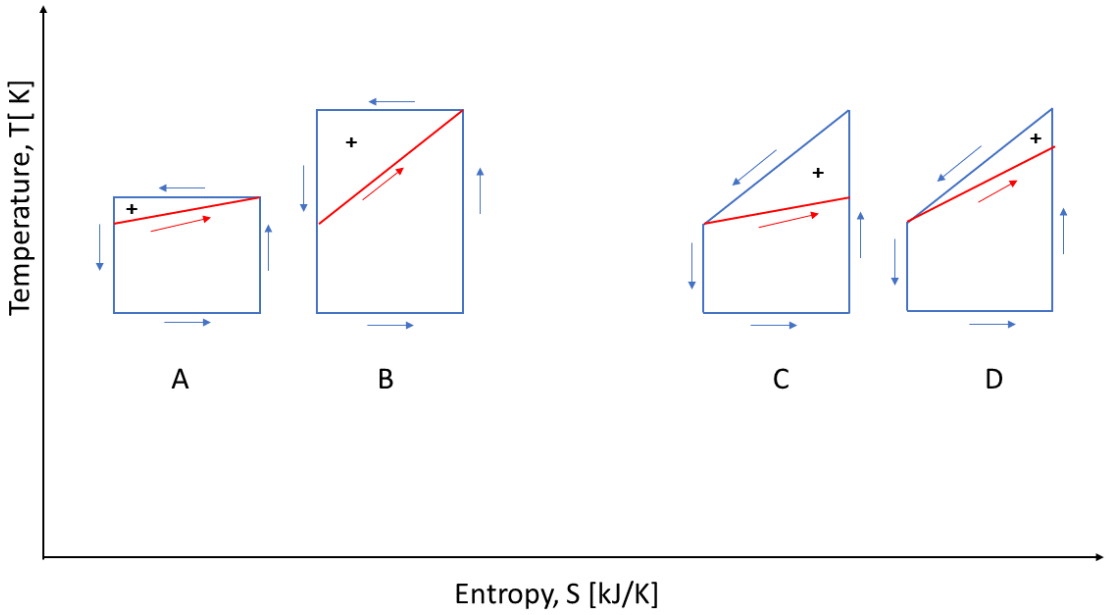

Figure 2: *Carnot and Lorentzen*

In general, most of the zeotropic mixtures experience a nonlinear temperature glide during condensation or evaporation. Tenary mixtures are, however more likely to attain linear temperature glides, compared to binary mixtures. The pinch point is where the temperature difference is the smallest during a heat exchange. If it exist a pinch point, it can only be located at the inlet or outlet of a heat exchanger when both fluids have linear temperature glides. In the case of parallel temperature glides, there are no pinch points. In that case, the irreversible losses can be reduced

to zero in theory by increasing the heat exchanger area. In the case of a nonlinear temperature glide, the pinch point could be located at any location within the heat exchanger. The nonlinear temperature glide can have a concave, convex, or s-shaped form. This means that there will be losses in the heat exchanger even if the heat exchanger area was increased to infinity. Radermacher & Hwang (2005)

Including the advantage of less loss in the condensers with the use of zeotrpic mixtures, there are other upsides as well. In recent years, there have been more interest regarding natural refrigerants such as ammonia, CO_2 and hydrocarbons. This is due to their zero ozone depletion potential (ODP), and negligible GWP. By applying mixtures, some of the individual shortcomings of each refrigerant could be reduced. Some of the main challenges of ammonia, is its toxicity. This toxicity can be reduced in a mixture. Flammability of hydrocarbons could also be reduced, and the high pressure demands for CO_2 could also be reduced if they were mixed with other refrigerants. Sarkar & Bhattacharyya (2009) CO_2 is a good fire extinguishing agent, and is therefore optimal to mix with hydrocarbons. Maccallum et al. (n.d.)

2.2 High temperature heat pump

The term HTHP is not formally defined and it is used differently in the literature. It exist, however, to some degree a common understanding in the literature of what a HTHP is. In most of the literature, a heat sink temperature of about 100 °C and a heat source around 50 °C is referred to as a HTHP. The only distinction between a regular heat pump and a HTHP are the heat sink and source temperatures. In every other way, the HTHP work according to the same principles as a regular heat pump. Arpagaus et al. (2018)

For regular heat pumps, common heat sources are such as outdoor air, heat from the ground or ground water. These sources have quite limited temperature range. HTHPs, on the other hand, often utilize waste heat from industrial processes as heat source, often obtaining larger temperatures. Waste heat temperatures can be in the range of 30 °C to 70 °C, which is desirable from an exergetic point of view as well. Waste heat from industrial processes occur as e.g. cooling liquid in chillers, waste water, hot compressed air etc. HTHPs often apply larger temperature lifts, compared to regular heat pumps. Arpagaus et al. (2018)

2.3 Cascade configuration

A cascade heat pump is made up of multiple single-stage vapor compression cycles. The cycles are linked in series with a counterflow heat exchanger, often called cascade heat exchanger, between each cycle. Figure 3 shows a simple sketch of a cascade heat pump consisting of two vapor compression cycles. The cascade heat exchanger serve as the condenser for the LS cycle, and as the evaporator for the HS cycle. That is, the LS cycle rejects heat for the HS cycle to absorb it in the cascade heat exchanger.

By applying such a configuration, it is easier to obtain large temperature rises. In a general heat pump, it is difficult to achieve large temperature rises and at the same time maintain a high COP.

In order to obtain larger temperature rise, larger compressor work is required as well. By applying a cascade configuration, the pressure ratio in each cycle is reduced, resulting in higher compression efficiency compared to a single-stage cycle. The cascade configuration is therefore advantageous when large temperature rises are to be obtained. AIKINS et al. (2013)

Another feature of the cascade configuration is that it allows different refrigerants to be used. because of this, the refrigerants used in the different stages can be selected to have advantageous characteristics for the specific stage. In the low stage, it is preferred to have a refrigerant that evaporates at low temperatures, but at relatively high pressures. At the same time, in the high stage it is optimal to have a refrigerant that condenses at a desired temperature and at a relatively low pressure. In that way, the over all pressure ratios are kept small while the temperature rise can be large. Moran et al. (2018)

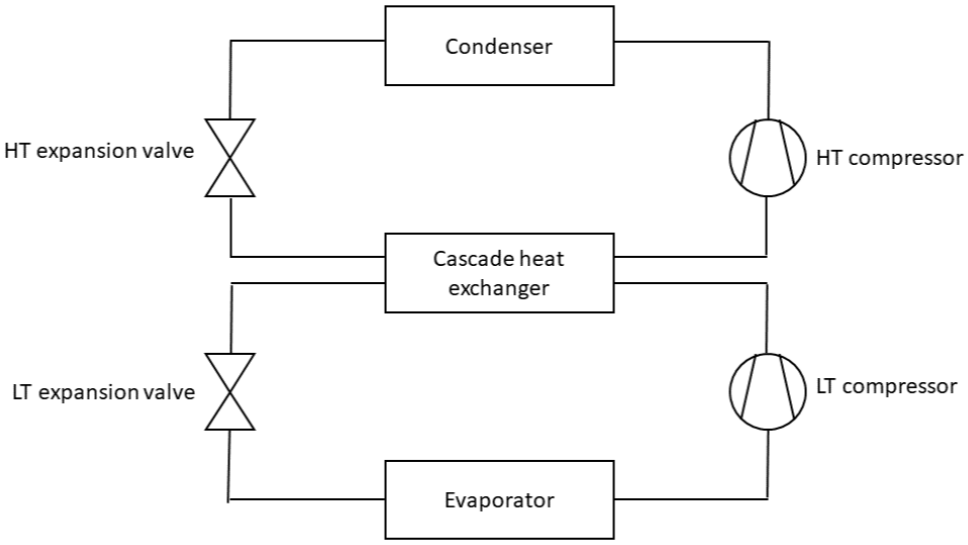

Figure 3: *Cascade HP*

2.4 PVT module

Solar energy is the most abundant energy source of the renewable energy sources, with an emitting rate of $3.8 \cdot 10^{23}$ kW, of which $1.8 \cdot 10^{14}$ kW reach the earth. Solar energy is available all over the world with no cost and it is non-exhaustible, hence it is a very promising energy source. The effect of solar energy as a energy source is determined by the solar radiation distribution and its intensity. These parameters are varying across the world, with Asian countries as the ones with highest potential to receive solar radiation. Kannan & Vakeesan (2016)

Photovoltaic (PV) systems consist of PV cells, which collect solar radiation and convert it to electricity. The part of the solar radiation that is not converted to electricity, will heat up the cells and increase the temperature. The PV conversion efficiency is inversely proportional with

the cell temperature, hence it is advantageous to keep the cell temperature low. To keep the cell temperature at a desired level, it is usual to use forced or natural air circulation to chill the cells. It is a cheap method, but at areas where the air temperature is higher than 20 °C it is less efficient. It is also possible to use water, which is a more expensive technique. Lamnatou & Chemisana (2017)

There are cases where the cooling fluid can be used in other practical applications, than just cool the PV cells. In those cases, photovoltaic thermal (PVT) solar collectors are applied. In these systems, PV collectors and solar thermal collectors are mounted together, and are able to produce both heat and electricity. Figure 4 shows an example of a simple PVT module. In this example, cold water coming from e.g. a TES oras waste heat from a consumer, enter the PVT system, absorb solar energy in the module and increase temperature. The hot water can be delivered back to the TES or to a consumer for direct use. At the same time, the cell temperature decrease and the conversion efficiency is maintained at a desirable level, for proper electricity production. The electrical energy can be directed directly to a consumer for use, or it can be stored in a battery, just as for the thermal energy. Lamnatou & Chemisana (2017)

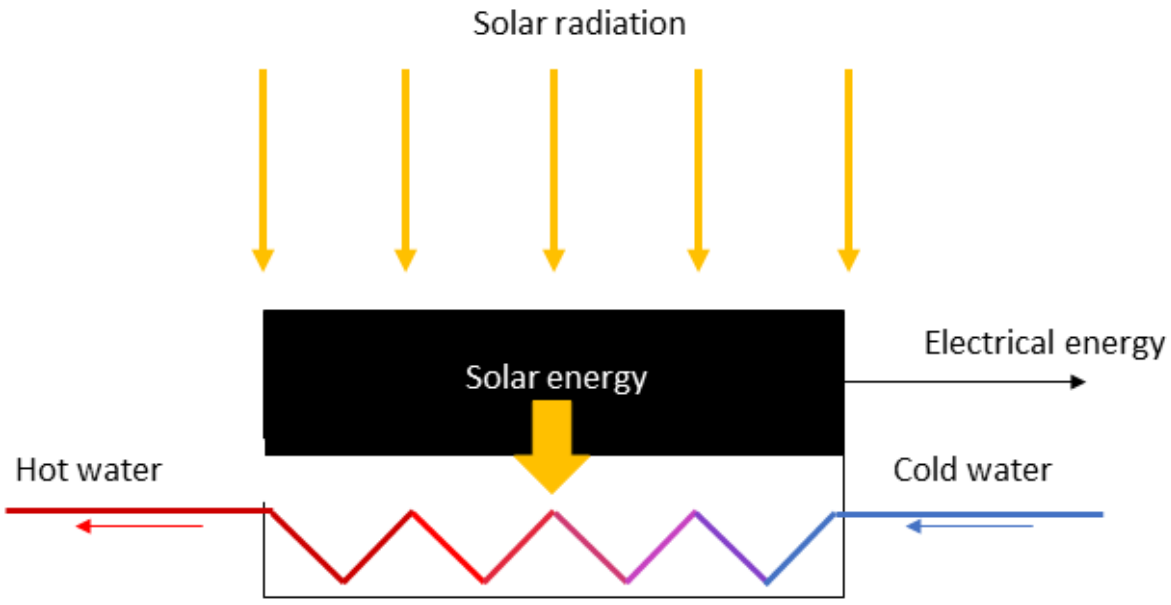

Figure 4: *PVT module*

Other qualities of the PVT system such as its capability to function unattended for longer periods of time, low maintenance cost, long effective life, high reliability and the fact that it consist of non-moving parts, result in a very promising technology. The main disadvantage of the PVT system is the cyclic time dependence, and the weather dependence, assuring an unstable production of heat and electricity. To be able to obtain stable production of electricity and heat, PVT systems is

required to integrate with energy storage systems, which will be discussed in the next section 2.5. Singh (2013)

2.5 TES

In a wide range of applications and industries the energy demand vary throughout a time period. Energy demands can vary from day to day, week to week and also from year to year. In order to match these varying demands, thermal energy storage system can be a helpful system. By integrating an energy system with a TES, multiple advantages arise, e.g. the reduction of energy costs, energy consumption, pollution and equipment size. This will assure a more energy efficient and more economic viable system. Dincer & Rosen (2011)

There are different ways of storing thermal energy. The physical processes are done by alternating either the sensible heat or the latent heat of a substance, or by a combination of the two. It is also possible to store thermal energy trough chemical processes. Jouhara et al. (2020) The objective of the systems is to store thermal energy when there is a surplus of heat, and to utilize the stored heat later when the demand is large. It is also possible to utilize TES in a strictly economic fashion. By producing heat and store it when it is cheap, the overall system becomes more economic viable. When the production takes place far away from the consumption, TES is also applicable and can enhance the overall heating system. Alva et al. (2018)

TES can store energy by cooling, heating, melting, solidifying, or vaporizing a material. The energy is absorbed in the TES, and released when the process is reversed. Cooling and heating go under the category sensible heat storage. This is done by increasing or decreasing the temperature of a material. The specific heat and density of the storage material is important parameters considering efficiency and volume size. This is seen from equation 1, where Q is the stored heat in the TES, ΔT is the temperature change, ρ is the density , V is the volume, and C_p is the specific heat of the storage material. Sensible TES systems normally use rocks, ground, or water as storage medium. Dincer & Rosen (2011)

$$Q = \rho \cdot V \cdot C_p \cdot \Delta T \tag{1}$$

Latent heat storage, on the other hand, store energy by changing the phase of materials, referred to as phase changing materials (PCMs). Melting, solidifying, or vaporizing are examples of latent heat storage. The specific heat of solidification/fusion or vaporization, and the melting, or boiling temperature of the storage material are important parameters for the system. Dincer & Rosen (2011) The phase often changes often from solid to a liquid when the energy is stored. The change from liquid to gas has the highest latent heat of phase change, but there is such a large change in volume of the storage material, which makes it less preferred. Both latent and sensible heat storage may be used with the same storage material.

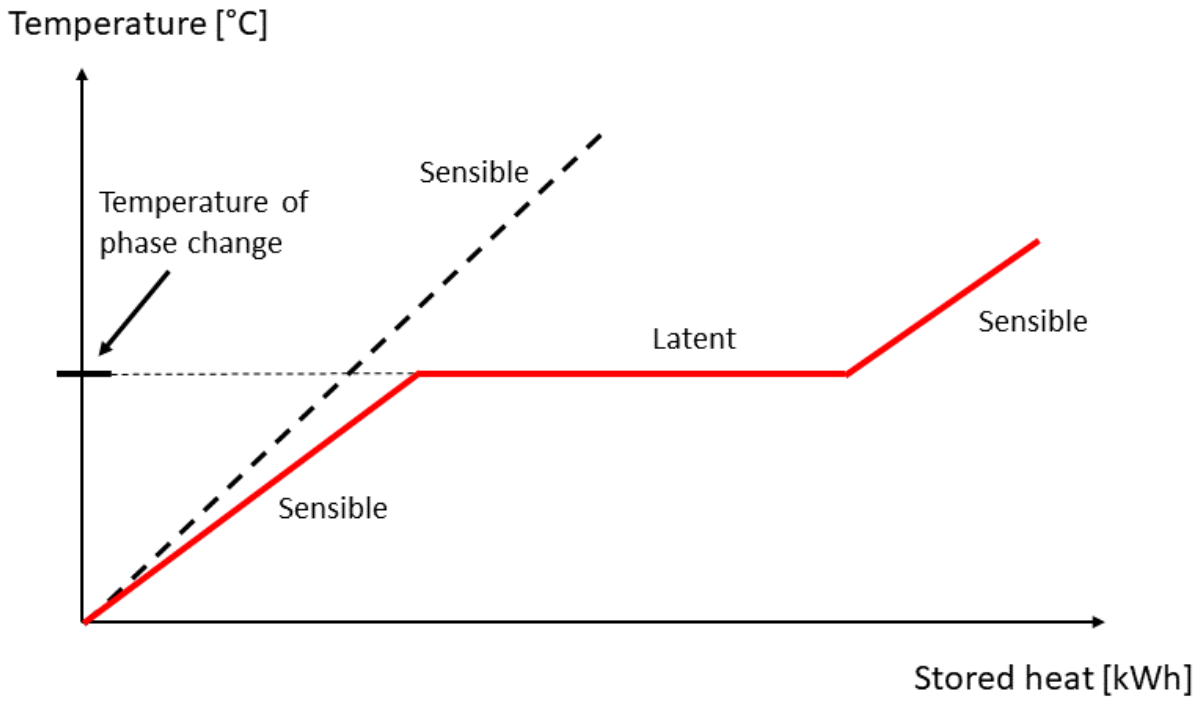

Figure 5: *TES*

Figure 5 shows an example of a TES using both latent and sensible heat storage. The x-axis show the thermal energy stored in the TES, and the y-axis shows the temperature of the storage material. As seen from the figure, during sensible heat storage, the stored heat increases proportionally with the temperature of the storage material. During latent heat storage, the material change phase at a constant temperature, while heat is absorbed. After the phase change, the temperature will again rise, if further heat is absorbed in the TES.

TES materials for latent heat storage is usually organic materials for thermal comfort in buildings. This is due to their solid-liquid phase change temperature is in the range of 18 °C - 30 °C, which is in the thermal comfort range for humans. Organic materials are also chemically stable, non-toxic, non-corrosive, and easily accessible in nature. Paraffin is the most common organic storage material. Inorganic materials, e.g. salts, on the other hand, usually have higher phase change temperatures, and are therefore more suitable for high temperature heat storage. Alva et al. (2018)

Latent TES systems are often more compact systems compared to sensible TES systems. This is due to latent heat being 50-100 times larger than sensible heat, resulting in higher energy storage density of latent heat storage materials. The more compact the system is, the cheaper it is. However, most of the sensible heat storage materials are low cost materials. Additionally, stable discharging temperatures are advantageous, making latent heat TES the better performer. On the other hand,

the thermal conductivity of latent heat storage materials tend to have poor thermal conductivities. Alva et al. (2018)

2.5.1 Borehole thermal energy storage

Borehole thermal energy storage (BTES) is an example of a sensible heat TES. It is one of the most promising technologies regarding long-term storage, both in terms of technologically and economic viability. BTES systems store energy in the ground below the surface. The material in the ground vary and can be f.ex. unconsolidated material, or solid rocks. The thermal conductivity of the ground is usually in the range of 1-5 $\frac{W}{m \cdot K}$ resulting in small heat losses in the storage. The heat losses are proportional to the surface of the storage, while the storage capacity is proportional to the volume, resulting in often large BTES systems with high storage capacities.

3 Method

3.1 General

Prior to the thesis, a project work was conducted, where different configurations were evaluated based on multiples variables such as COP, and volumetric heat capacity (VHC). Based on this evaluation, a cascade configuration was evaluated as a suitable configuration for a HTHP. Based on this, the cascade configuration is selected in this thesis as well, but without the same refrigerants. The main objective of the thesis is to investigate the performance of a HTHP in an integrated energy system, that can provide heat at above 100 $°C$, with a temperature rise of 50 $°C$.

Most of the models and principles of the simulation approach is collected from Ryssdal (2020). In this thesis an already working Matlab model was used, but some main parts were changed and/or updated, in order to fit other aspects of the performance of the heat pump. As in Ryssdal (2020), weather data was collected from Meteonorm, but in this thesis the weather data was collected from Oslo, Norway. The weather data that is used in the model is ambient temperatures and solar irradiance. The ambient temperatures forms the basis of the heat demand that is to be met by the energy system, and the solar irradiance is deciding the available power to the compressor and the temperature of the heat source used in the heat pump.

As in Ryssdal (2020), a base demand of 50 kW was chosen to represent the demand for water heating. This value is independent of the ambient temperatures and is therefore constant throughout the year. In addition to the water heating demand, a space heating demand is assumed to increase with 10.25 kW for every ambient temperature degree below 15 $°C$. The demand is calculated according to equation 2, where T_a is the ambient temperature in $°C$, and given that this temperature is below 15 $°C$.

$$Q_{demand} = 50 + 10.25 \cdot (15 - T_a) \qquad [kW] \tag{2}$$

3.2 PVT model

The PVT model used in this thesis was accessed from Herrando et al. (2019). The panels that are being considered in this thesis, is a commercial sheet-and-tube PVT collector, which is a ECOMESH from EndeF Engeneering. *Panel Solar Híbrido ECOMESH - ENDEF* (n.d.) There are different methods to estimate the performance of a PVT collector. ASHRAE and ISO are two methods that are considered in the paper by Herrando et al. (2019), but the ISO method is chosen here in this thesis. In the ISO method, the thermal efficiency of the PVT collector is calculated at different mean fluid temperatures and ambient temperatures. This equation is shown in equation 3.

$$\eta_{th} = \eta_o - a_1 \cdot T_r - a_2 \cdot I_t \cdot T_r^2 \qquad [-] \tag{3}$$

$$T_r = \frac{T_{fm} - T_a}{I_t} \qquad [K] \tag{4}$$

In equation 3, η_o is the optical efficiency which is a measurement of how much of the incident radiation collected by the receiver is converted into thermal energy. López-Martín & Valenzuela (2018) a_1 is the heat loss coefficient which accounts for linear heat loss variation in $[\frac{W}{m^2 \cdot K}]$, while a_2 is the heat loss coefficient accounting for the quadratic heat loss variation in $[\frac{W}{m^2 \cdot K^2}]$. T_r is the reduced temperature which is calculated in equation 4, and here T_{fm} is the mean temperature of the fluid that is passing through the PVT collector in $[K]$, T_a is the ambient temperature in $[K]$, and I_t is the incident radiation in $[\frac{W}{m^2}]$.

The electrical performance model of the PVT collector is also collected from Herrando et al. (2019). The electrical efficiency varies linearly with the cell operating temperatures, as mentioned earlier in section 2.4. The electrical efficiency of the PVT module is calculated according to equation 5.

$$\eta_{el} = \eta_{ref} \cdot (1 - \beta_0 \cdot (T_{PV} - T_{ref})) \qquad [-] \tag{5}$$

In equation 5, η_{ref} is the reference module efficiency at a PV cell temperature of 25 $^\circ C$, and a solar irradiance of 1000 $\frac{W}{m^2}$, T_{ref} is the reference temperature of the PV cell in $[K]$, and β is the temperature coefficient of the PV module in $[1/K]$.

In equation 6 and 7 the total thermal and electrical energy produced by the PVT module is calculated, respectively. In these equations A_{PV} is the total surface area of the PVT module, and the factor of $\frac{1}{1000}$ is used in order to obtain kW instead of W.

$$E_{th} = \frac{\eta_{th} \cdot I_t \cdot A_{PV}}{1000} \qquad [kW] \tag{6}$$

$$E_{el} = \frac{\eta_{el} \cdot I_t \cdot A_{PV}}{1000} \qquad [kW] \tag{7}$$

In table 1, the constants used in the equations 3 - 7 are summarized and displayed.

Specifications	**Value**
Optical efficiency, η_o	0.51 [−]
Linear heat loss coefficient, a_1	4.93 $[\frac{W}{m^2 \cdot K}]$
Quadratic heat loss coefficient, a_2	0.021 $[\frac{W}{m^2 \cdot K^2}]$
Reference module efficiency, η_{ref}	0.147 [−]
Reference PV cell temperature, T_{ref}	25 $[°C]$
Surface area of PVT module, A_{PV}	4000 $[m^2]$
Temperature coefficient, β_0	-0.0045 $[1/K]$

Table 1: *Caption*

3.3 TES model

The TES model is collected from Ryssdal (2020). As seen in figure 11, the PCM storage is connected to the district heating system. For every hour the demand from the district heating system is calculated, and based on this, the action of the TES is decided. If the heat pump is producing more heat than necessary according to the demand, the excess heat is stored in the TES. If the heat pump is unable to cover the heat demand, the TES is discharged and supplying heat to the district heating system along with the heat pump. If the heat production from the heat pump is exactly the needed the heat to cover the demand, the thermal capacity remains the same. The charging/discharging efficiency is 90 %, i.e., 10 % heat is lost during every charging/discharging action. The maximum storage capacity is 1000 kWh.

3.4 Battery model

Just as for the TES model, the battery model is also collected from Ryssdal (2020). The principle of the battery storage is quite similar to the TES. Instead of storing thermal energy, the battery stores electric energy. For every the power required by the compressors are calculated, and based

on this the the action of the battery storage is decided. If the power produced by the PVT system exceed the power required by the compressors, the excess power is stored in the battery. In the opposite case where the power production is insufficient to cover the demand, the power stored in the battery is supplying the compressors. If the demand is equal to the power production, the capacity is unchanged. The charging/discharging efficiency is set to 80 %.

3.5 BTES model

The BTES model is quite similar to the TES model. It is a simplified and general model, where the objective of the model is to increase the temperature to a satisfactory level, when the PVT system is unable to do so, due to low solar irradiance. There is not chosen a specific length of the borehole, nor a specific material of the bore hole heat exchanger (BHE). Just as in the TES model, for every hourly iteration, the energy inserted into or extracted from the BTES system is calculated. Then the capacity of the BTES is calculated and used in the next iteration.

The fluid temperature out of the PVT system is essential in this model and controls the discharge/charge decision. A temperature of 45 $^{\circ}C$ is sat as a reference temperature of the evaporator inlet temperature. This temperature is the required temperature to meet the demanding energy from the evaporator. Hence, if the fluid temperature out of the PVT system is higher than this reference temperature, the excess heat is directed to the BTES. If the fluid temperature out of the PVT system is, on the other hand, lower than the reference temperature, heat is extracted from the BTES. The fluid extracts the amount of heat required to obtain the reference temperature, given that this amount is available in the BTES. The energy extracted or inserted in the BTES is calculated by equation 8.

$$Q = \dot{m} \cdot C_p \cdot (T_{pvt,out} - T_{e,in,ref}) \qquad [kW] \tag{8}$$

Here is $\dot{m}$ the mass flow of the fluid entering the BTES in $[\frac{kg}{s}]$, C_p is the spesific heat of the fluid in $[\frac{kJ}{kg \cdot K}]$, and $T_{pvt,out}$ is the temperature of the fluid entering the BTES, and $T_{e,in,ref}$ is the fluid temperature exiting the BTES in $[K]$.

3.6 Heat pump model

3.6.1 Configuration

The heat pump was modelled as a cascade heat pump, just as in the project work. The choice of the particular configuration was described in the project work, which was a preliminary report to the master thesis. An illustration of the configuration is shown in figure 6. The fluid entering the evaporator is a water/ethanol mixture in order to prevent freezing. The mixture has a 90/10 mixture mass fraction and a freezing point of ... which assure a safety margin, so the fluid doesn't freeze during the cooling. The inlet temperature of the fluid is marked as 45 $^{\circ}$ in the figure, which represent the ideal operation.

The low-stage refrigerant, which is propane is heated by the water/ethanol mixture. After the evaporation (1), the refrigerant is entering the low stage (LS) internal heat exchanger (IHX). The internal heat exhcanger is applied in order to avoid liquid entering the compressor (2). The LS compressor compresses the refrigerant from about 1220 kPa to 2440 kPa (3). Thereafter, the refrigerant is condensing at a temperature of about 67 °C (4), where at the same time, the mixture in the high stage (HS) cycle is being evaporated (7). After the LS condenser, the refrigerant is being cooled in the IHX (5), and lastly it is expanding isenthalpic in the LS expansion valve (6), before it enters the evaporator again.

As mentioned, the mixture in the high stage is evaporated in the cascade heat exchanger at a pressure of about 690 kPa. This is equivalent to a temperature glide from 52 °C to 60 °C. The HS follows the same procedure as in the LS according to compressing, cooling in the IHX and expansion. The mixture is condensing at a pressure of about 1800 kPa, which corresponds to a inlet and outlet temperature of about 110 °C and 80 °C, respectively. During this condensation, water is absorbing the heat and increase the temperature form 60 °C to 100 °C. It is to be noted that the refrigerant and the hot water has a temperature glide of 30 °C and 40 °C, respectively.

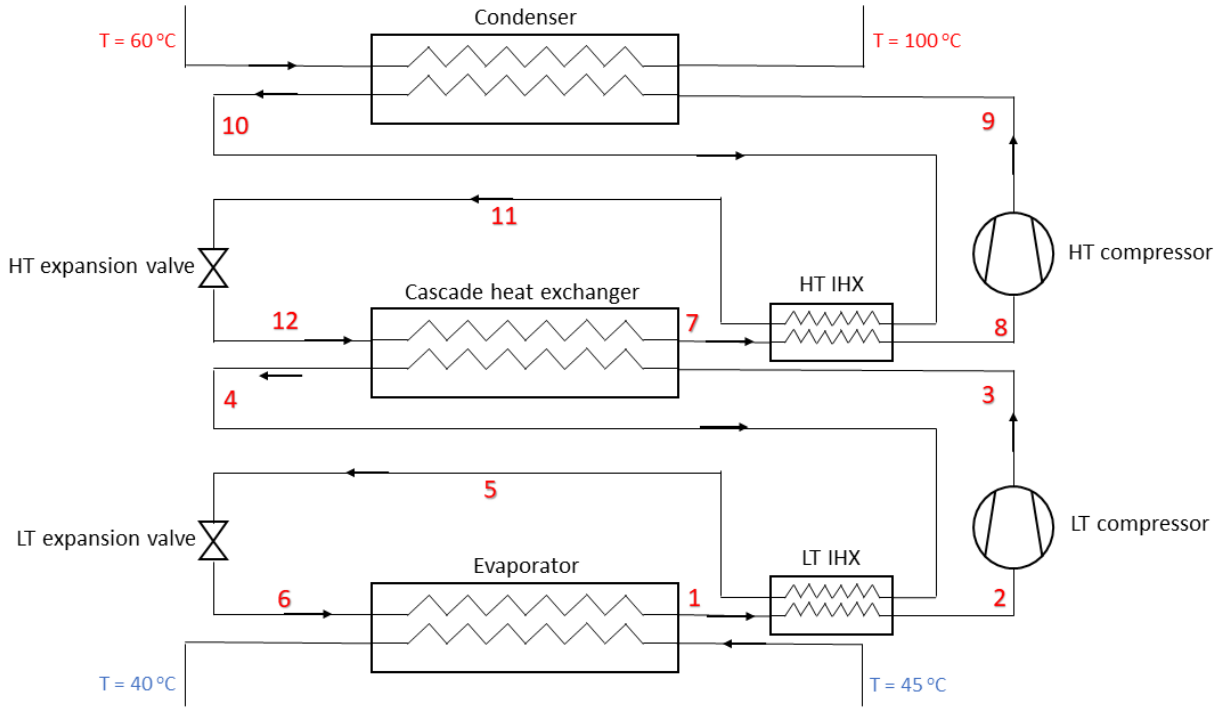

Figure 6: *Configuration of HP*

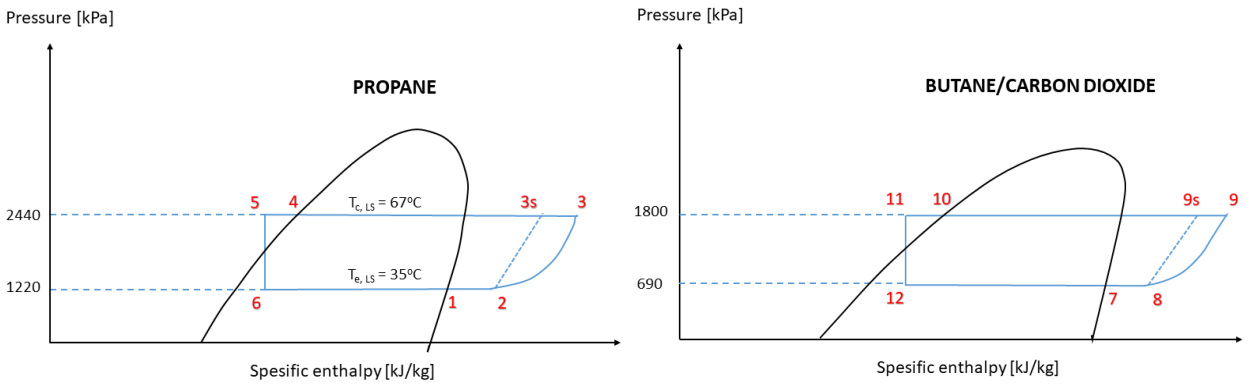

(a) *Propane* **(b)** $CO_2/Butane$

Figure 7: *P-h diagrams*

3.6.2 Refrigerant selection

Sarkar & Bhattacharyya (2009) did an assessment of CO_2/butane blends, which was discussed in 1.2.2. The assessment showed that the blends performed better than single component refrigerants. Given that the literature review showed such promising results for the CO_2/butane mix and the fact that butane was used in the project work, prior to this thesis, the CO_2/butane mix was selected as the refrigerant in the high stage. There was not conducted a optimal mixture ratio analysis. A desire to keep the pressures low and at the same time have a proper temperature match in the condenser, was the basis of the choice of 5 % mass fraction of CO_2 in the mixture. In figure 8, the condensation process i showed at a pressure of 1800 kPa. The figure shows a relatively good temperature match, and is therefore the chosen high stage refrigerant. In the low stage, based on the literature review conducted in the project work, propane was chosen. Propane is widespread in the literature, and have good qualities as a refrigerant as discussed in the literature review in the project work.

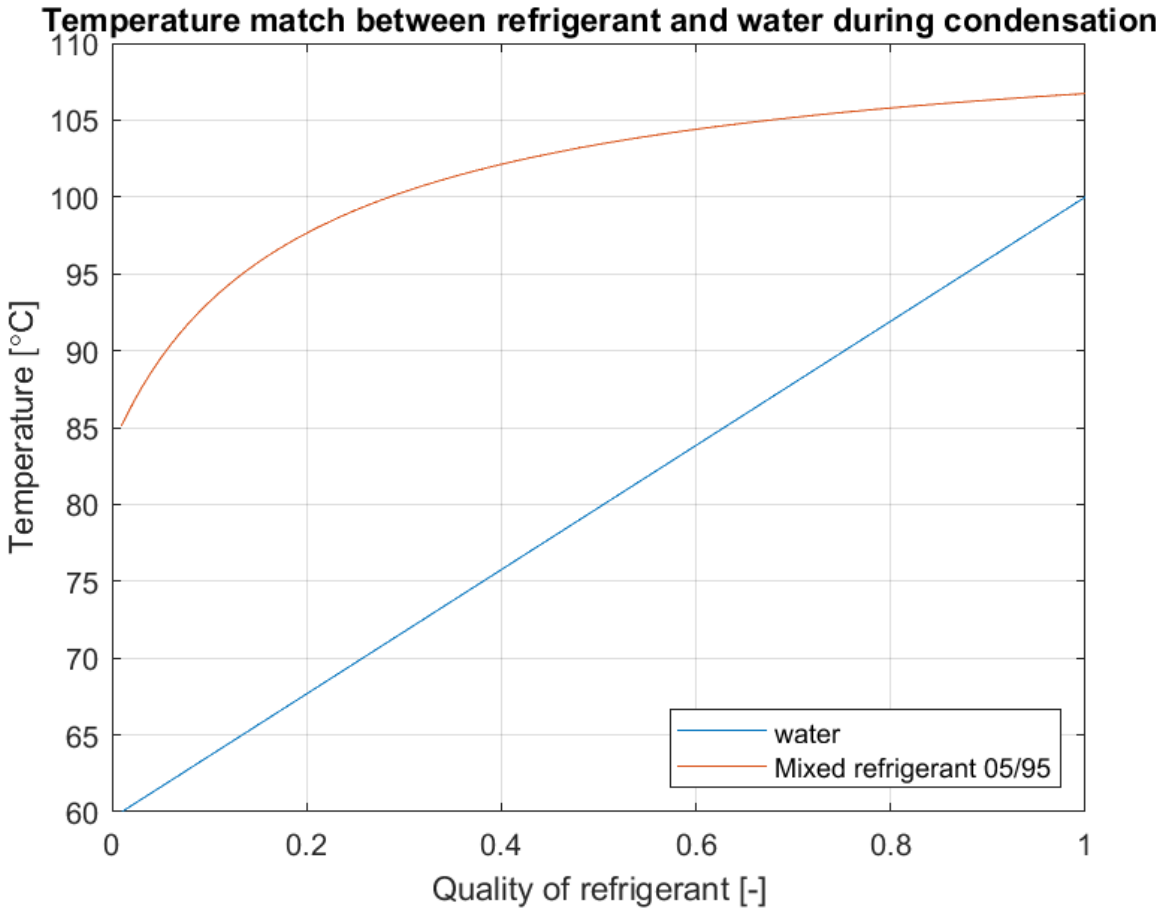

Figure 8: *Condensation process*

3.6.3 Condenser model

Due to the nonlinear temperature glide throughout the condenser, a model had to be created in order to solve the condensing temperature glide. Figure 9 shows a sketch of the temperature change along the condenser for the water to be heated as well as the refrigerant that is condensing. In this sketch, the temperature range is only divided in ten segments, but it is just to illustrate the process. It is desirable to obtain the logarithmic mean temperature difference (LMTD) of the heat exchanger. The condenser is therefore divided in segments in order to approach a linear temperature glide in each segment. When there is an approximate linear temperature change in each segment, equation 9 can be utilized. A for loop is created to divide the condenser in twenty segments. At every iteration the LMTD is calculated from both equation 9 and 10.

$$LMTD_c = \frac{(T_{c,in} - T_{w,out}) - (T_{c,out} - T_{w,in})}{log(\frac{T_{c,in} - T_{w,out}}{T_{c,out} - T_{w,in}})} \qquad [K] \tag{9}$$

$$LMTD_c = \frac{Q}{U \cdot A} \qquad [K] \tag{10}$$

$T_{c,in}$, $T_{c,out}$, are the refrigerant temperature entering and exiting each segment of the condenser in $[K]$, while $T_{w,in}$ and $T_{w,out}$ are the water temperature entering and exiting each segment also in $[K]$. U is the heat transfer coefficient in $[\frac{W}{m^2 \cdot K}]$, A is the area of each segment in $[m^2]$, and Q is the heat transfer at each segment in $[W]$.

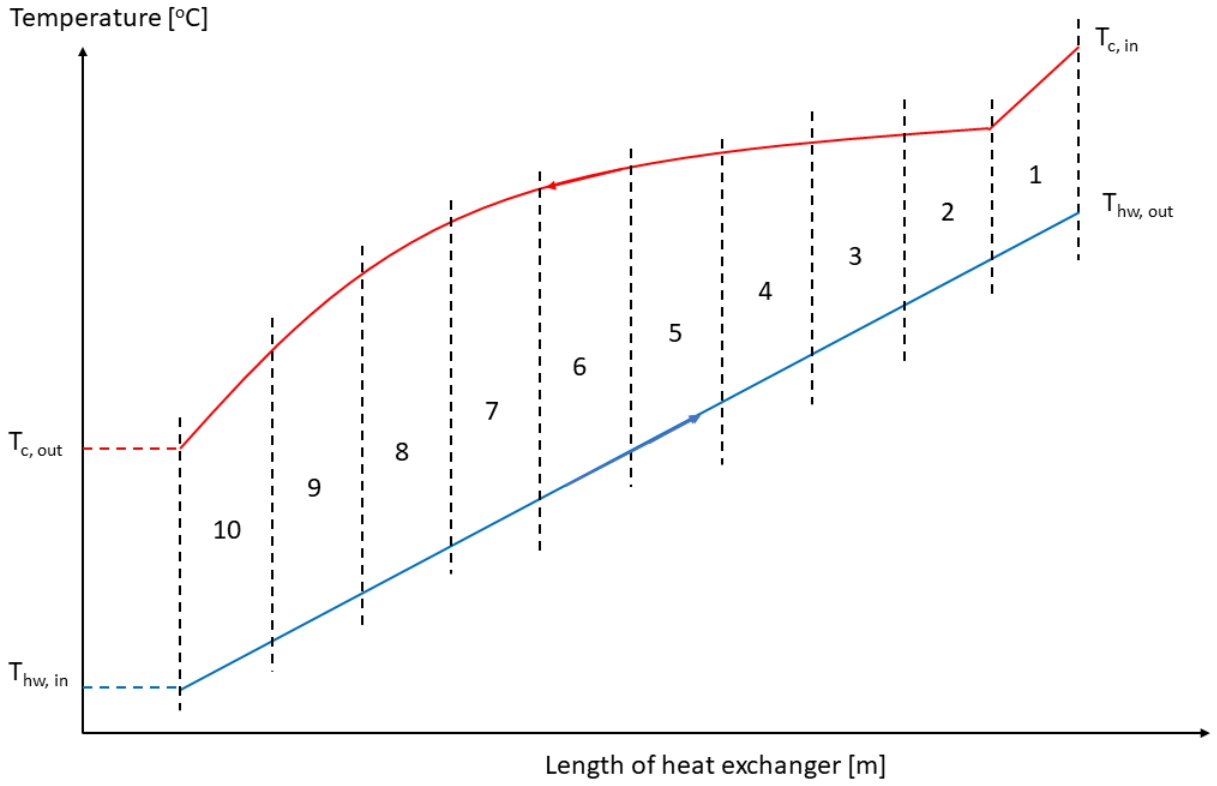

Figure 9: *Condenser model*

3.7 Algorithm

The model of the BTES system and PVT system was created separately from the main script. Given that the PVT system and BTES system is directly connected and are both accountable for the evaporator inlet temperature, both models were created in a single script. When the script was functioning satisfactory and producing evaporator inlet temperatures, the models were added to the main script.

In addition to the script containing the PVT and BTES systems, a script was created to dimension the heat pump. The heat pump was simulated for one hour, where the pressure in the condenser,

as well as all the temperatures in and out of the heat exchangers were assumed. This was done to calculate the area of the heat exchangers, as well as the size of the compressors, that was going to be used in the main script. The heat transfer coefficient that were used for the heat exchangers were collected from *Engineering ToolBox* (2020) and are displayed in table 2

	U-value $[\frac{W}{m^2 \cdot K}]$
Condenser	1400
Evaporator	1600
Cascade HX	1800

Table 2: *Heat transfer coefficients*

The simulation process starts with weather data from Oslo, Norway being imported to excel from the program Meteonorm, and then Matlab collects these data. The entire system is simulated for every hour throughout a year, which is done by a for-loop. This leads to 8760 iterations. For every hour, the PVT, BTES, TES, battery and HP system is simulated. All variables necessary to describe the operation of these systems are calculated in every iteration, in order to evaluate their performance.

3.7.1 PVT/BTES algorithm

The main objective of this algorithm is to calculate the cold water temperatures in to and out of the evaporator. This is a greatly simplified model compared to real systems. The main focus is to evaluate the performance of the heat pump with transient heat sink temperatures. Consequently, the heat pump algorithm contains less simplifications than the PVT & BTES algorithm.

The algorithm used to obtain the water/ethanol mixture temperature out of the PVT system uses the bisection method which is done also for the evaporation temperature, which is explained in section 3.7.2 below. An initial temperature is used to calculate the thermal and electric energy produced by the PVT system according to equation 3 - 7. A new temperature is then calculated based on the obtained thermal energy. The difference between the old and new temperature is then subtracted from the old temperature. This process is repeated until the difference between the two temperatures are less than 0.1 K.

This temperature is then checked against the temperature of the water/ethanol mixture entering the PVT system. If the exiting temperature is less than the inlet temperature plus 1 $°C$, the inlet temperature is reduced and the process of calculating the outlet temperature, as explained in the paragraph above, is repeated. This process is done with a while loop where the inlet temperature is reduced with a single degree in every iteration. The while loop keeps iterating until the outlet temperature become larger than the inlet temperature plus 1 $°C$ or become less than the natural soil temperature minus 1 $°C$. The temperature that are calculated is then used in further calculations of heat, as explained in section 3.5.

3.7.2 Main script

Prior to the for-loop in the script, the necessary weather data are imported from Meteonorm, and then arrays are pre-allocated for the variables used in the code. Inside the for-loop the heat and power generated by the PVT system is calculated first. This particular algorithm is described closer in section **??**. Based on this, the cold water temperature is calculated and the initial evaporation temperature is obtained. Furthermore, the heat demand is calculated according to equation 2. When the initial evaporation temperature, heat demand, and available power is calculated the heat pump loop begins. A flowchart of the simulation process of the heat pump loop is shown in figure 10.

The heat pump loop start with initial guesses of the evaporation temperature and outlet condenser temperature. Based on this the pressure, temperature, and enthalpy is calculated in every stage, (1)-(12). The isentropic and volumetric efficiency of the compressors are important parameters when obtaining the state properties. The isentropic efficiency is used to obtain the enthalpy at the compressor outlet in both stages, and the volumetric efficiency is used to obtain the mass flow rate in both stages. The efficiencies are calculated by equation 11 and 12. Just as in the project work, these equations were collected from Ryssdal (2020). In these equations, π is the pressure ratio of the outlet and inlet pressure of the compressor.

$$\begin{aligned}\eta_{is} = &-0.00000461 \cdot \pi^6 + 0.00027131 \cdot \pi^5 - 0.00628605 \cdot \pi^4 + 0.07370258 \cdot \pi^3 \\ &-0.46054399 \cdot \pi^2 + 1.40653347 \cdot \pi - 0.87811477 \qquad [-]\end{aligned} \tag{11}$$

$$\lambda = 0.0011 \cdot \pi^2 - 0.0487 \cdot \pi + 0.9979 \qquad [-] \tag{12}$$

Subsequently of the calculation of the state properties, the mass flow rates in both LS and HS are calculated based on the enthalpy values as seen in equation 13 and 14. Initially, the mass flow rate in the LS cycle is set to maximum flow rate allowed by the compressor size, which is according to equation 13. The mass flow rate in the HS cycle is based on the energy conversion in the cascade heat exchanger. Since the amount of heat rejected by the LS cycle must be equal to the amount of heat absorbed by the HS cycle, the mass flow rate in the HS cycle is calculated according to 14. If mass flow rate in the HS cycle exceed the maximum flow rate allowed by the compressor size, the speed of the LS compressor is reduced until the mass flow rate in the HS cycle is the same as the maximum mass flow rate.

$$\dot{m}_r = \frac{\rho_{in} \cdot V_{comp} \cdot \lambda}{3600} \qquad [\frac{kg}{s}] \tag{13}$$

$$\dot{m}_{r,hs} = \dot{m}_{r,ls} \cdot \frac{h_3 - h_4}{h_7 - h_{12}} \qquad [\frac{kg}{s}] \tag{14}$$

In 13, ρ_{in} is the density of the refrigerant entering the compressor in $[\frac{kg}{m^3}]$, V_comp is the compressor size in $[\frac{m^3}{h}]$ and λ is the volumetric efficiency. In 14, $m_{r,ls}$ is the mass flor water in the LS cycle in

$[\frac{kg}{s}]$, while h_3, h_4, h_7, h_{12}, are the enthalpies in $[\frac{kg}{s}]$ in the states 3, 4, 7 and 12, in figure 7. Once the mass flow rates, and enthalpy values are obtained, the power consumption of the compressors, the condensation heat and then COP are obtained.

The evaporation temperature and condensation temperature range are implicit functions. All the state properties are dependent on these temperatures. The evaporation and condensation heat are in turn, dependent on the state properties. The water temperature out of the condenser and evaporator are obtained from the condensation and evaporation heat. The evaporation temperature and condensation temperature range are, in turn, dependent on the water outlet temperatures of the evaporator and condenser, respectively. Hence, in order to solve the evaporator temperature and condenser temperature range, a while loop is created.

In the while loop the LMTD in the tenth segment of the condenser is the basis for solving the condenser temperature range. A initial value of the LMTD and the condenser pressure is guessed and used to calculate the state properties and the evaporation and condensation heat. The LMTD is then calculated in all segments according to both 10 and 9. The condenser pressure is then adjusted until the LMTD values in the tenth segment, calculated by both equations, differ with less than 0.1 K. If the LMTD obtained from 10 is larger than the LMTD obtained from 9 the pressure is increased by a certain amount, while the pressure is reduced if the case is reversed. In order to make the loop converge, the amount of pressure that is reduced or increased, is adjusted. If the difference between the two LMTD-values differ in sign from an iteration in the while loop to the previous iteration, the amount of pressure change is divided by two. In that way, the pressure is adjusted until the LMTD-values in the tenth segment, obtained from the two equations 10 and 9, differ with less than 0.1 K.

The evaporation temperature is also adjusted. An initial evaporation temperature is guessed and at each iteration of the while loop, the evaporation temperature is calculated according to 15. The difference between the old and new evaporation temperature is then divided by two and subtracted from the old temperature and used in the next iteration. The temperatures in the cascade heat exchangers are calculated based on the evaporation temperature and condensing temperature glide. The outlet temperature in the high stage is mean temperature between the evaporation temperature and the mean condensation temperature minus 3.5 $^{\circ}C$. The condensing temperature in the low stage is 7 $^{\circ}C$ higher than the outlet temperature in the high stage.

$$T_e = \frac{T_{cw,out} \cdot e^{\frac{T_{cw,in}-T_{cw,out}}{LMTD_{evap.}}} - T_{cw,in}}{e^{\frac{T_{cw,in}-T_{cw,out}}{LMTD_{evap.}}} - 1} \qquad [K] \tag{15}$$

Posterior of the while loop, the heat pump has obtained correct state properties, and the load operation is to be decided. Since there is an uneven supply of electric power that is available for the compressors to utilize, it is necessary to take this into consideration, and regulate some variables.

It is desirable to make the heat pump run on part load as little as possible. Therefore the heat pump is running on full load as long as there is enough available power and the maximum capacity of the TES is not reached. The heat pump will produce heat to the TES and the district heating system, when there is excess heat due to low demands. When the TES is full, the heat pump will be turned off until the TES capacity is insufficient to cover the demand.

The power demand is compared to the available power from the PVT system and the battery. If the available power is larger than the power demand, the properties obtained in the while loop become the output of the algorithm. If, on the other hand, the available power is insufficient to meet the power demands, the heat pump will run on part load. This is done by reducing the speed of the compressor. Firstly the ratio between heat demand and maximum heat capacity will be calculated, and the compressor speed will be regulated so the heat pump only covers the heat demand. The heat pump loop is then run again with the reduced compressor speed.

If the available power is still insufficient to meet the power demands from the compressors, the compressor speed is further reduced. The compressor speed is reduced with 20 % until the available power is sufficient to meet the power demand, or until the load ratio is lower than 20 %, where the heat pump is shut off. When the proper state properties and power consumption is obtained, the heat that is sent to the district heating and/or TES is calculated. If the heat pump is shut off, the evaporation and condensation temperatures will be given the same value as the previous iteration in order to have proper initial values in the next iteration.

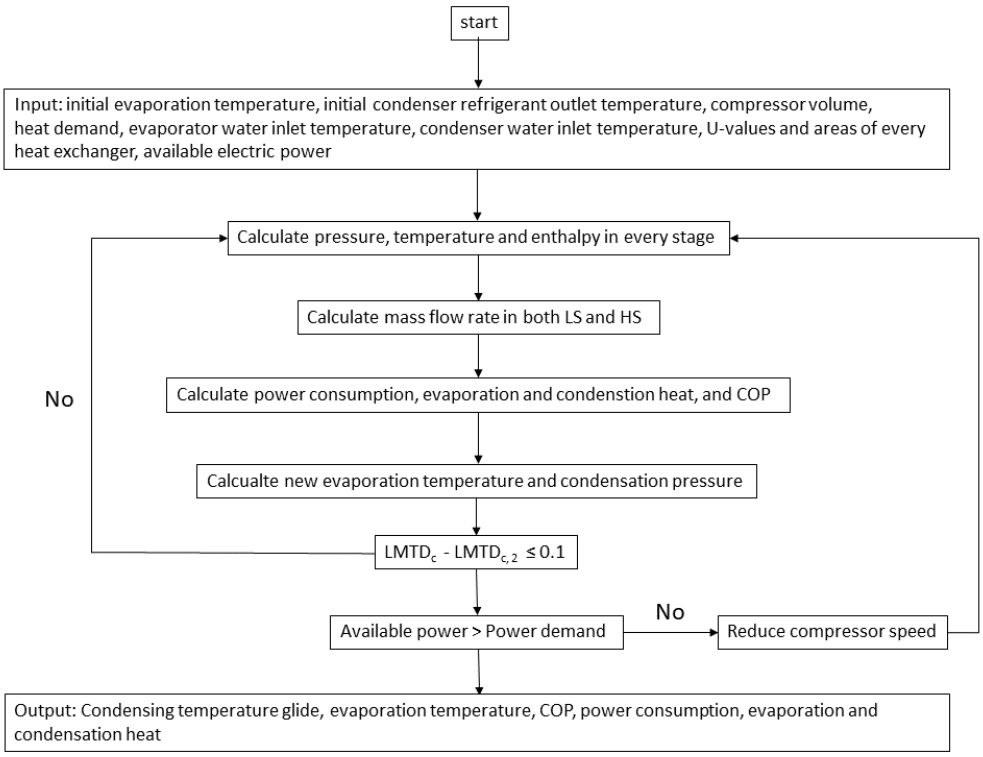

Figure 10: *Heat pump algorithm*

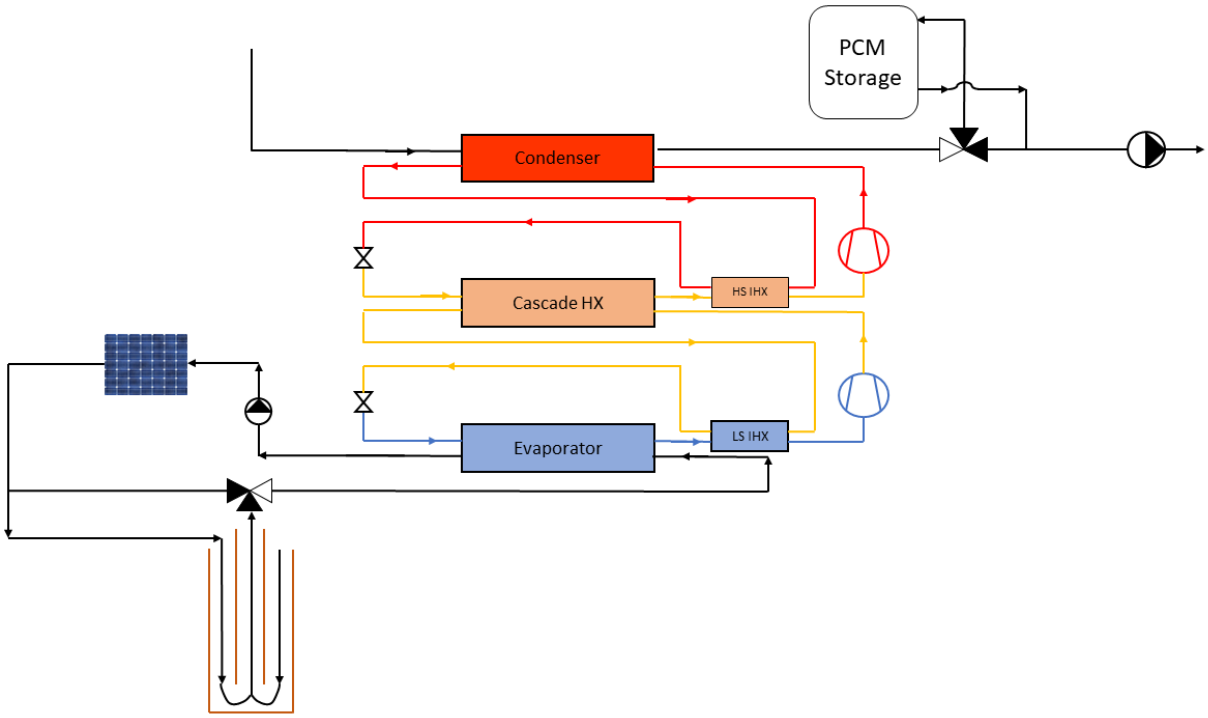

Figure 11: *Integrated energy system*

4 Results

The results in this thesis bear the mark of a malfunctioning code. During most of the work and testing of the code, an error occurred numerous times. In figure 12, a screenshot of the error message is shown. During testing of the code, this message frequently appeared, often at different iteration points, making it very difficult to debug and locate any errors in the code. Without a knowing what exactly the problem is, a suspicion is that the software runs out of RAM, due to the many iterations and calculations. Nevertheless, the code runs very slow compared to the code developed in the project work and the code in Ryssdal (2020).

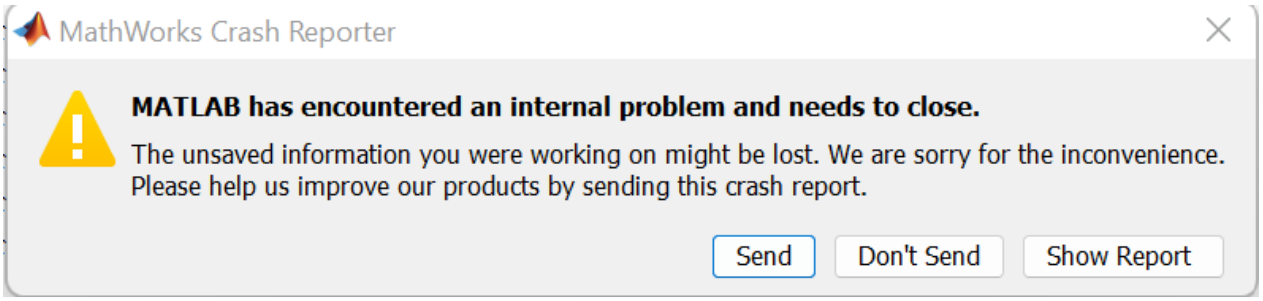

Figure 12: *Error message*

Even though it seemed like Matlab was struggling to process the code, there were found some malfunctions in the code as well. The algorithm explained in section 3.6.3, could not converge when the heat pump operated on part load. It seemed like for the lmtd-values to be the same, the pressure needed to be too low which was not functioning in the code. The code was unable to simulate the entire year, and even if the code was able to run at all iterations, this would take a very long time. Therefore the results will be mostly from the summer months, and the other parts of the year with part load operation will be discussed based on the simulation of the PVT system and BTES system.

4.1 PVT and BTES performance

4.1.1 Year

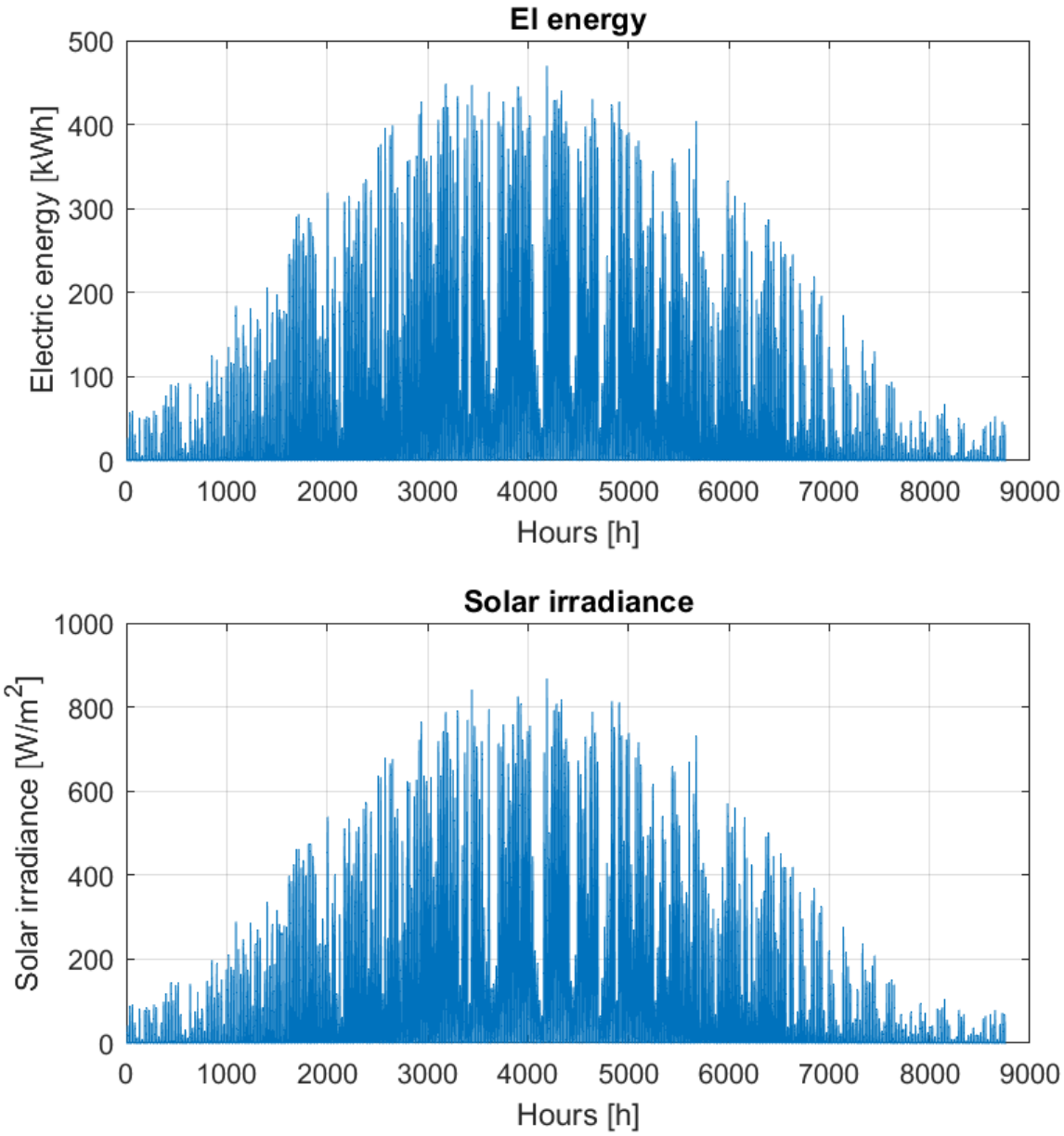

Figure 13: *Solar irradiance and electric energy produced by the PVT system*

Figure 13 shows the electric energy produced by the PVT system, and the solar irradiance over the course of a year. It is clear that the solar irradiance is increasing from January until summer, and

then decreasing during autumn and winter. However, there are large fluctuations during all seasons. The highest solar irradiance values are around 800 $\frac{W}{m^2}$. The electric energy produced by the PVT is following the same trends as the solar irradiance, and achieves around 450 kWh in certain hours throughout the year.

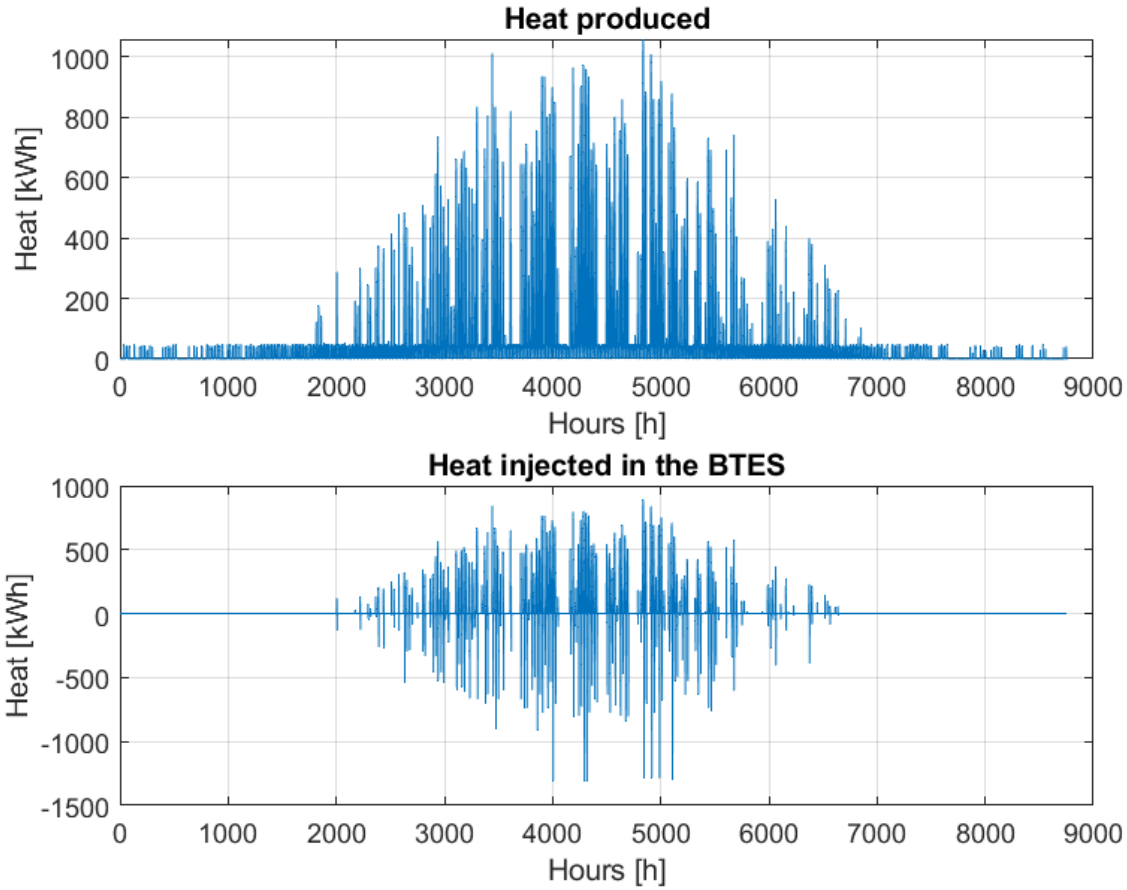

Figure 14: *Heat produced by the PVT system and heat injected into the BTES*

Figure 14 shows the heat produced by the PVT system during, and the amount of heat injected into the BTES during the year. For the first and last two thousand hours, the heat produced by the PVT system is fairly consistent when it is nonzero. During this period, the PVT system produce around 40-50 kWh, when the production is nonzero. In the summer however, there larger fluctuations, and the production reach up to around 1000 kWh in certain hours. There are a clear correlation between the two graphs; during the first and last two thousand hours of the year, the heat injected in the BTES is zero or close to zero. Almost all of the heat that is produced by the PVT system is directed directly to the evaporator during this period. During the summer, fluctuations in the graphs for the heat injection are large. The largest values are around 700-800 kWh, while the lowest values are around -1300 kWh. When the values in this graph are negative, it means heat is extracted from the BTES. This means, that for some hours, around 1300 kWh is extracted from

the BTES.

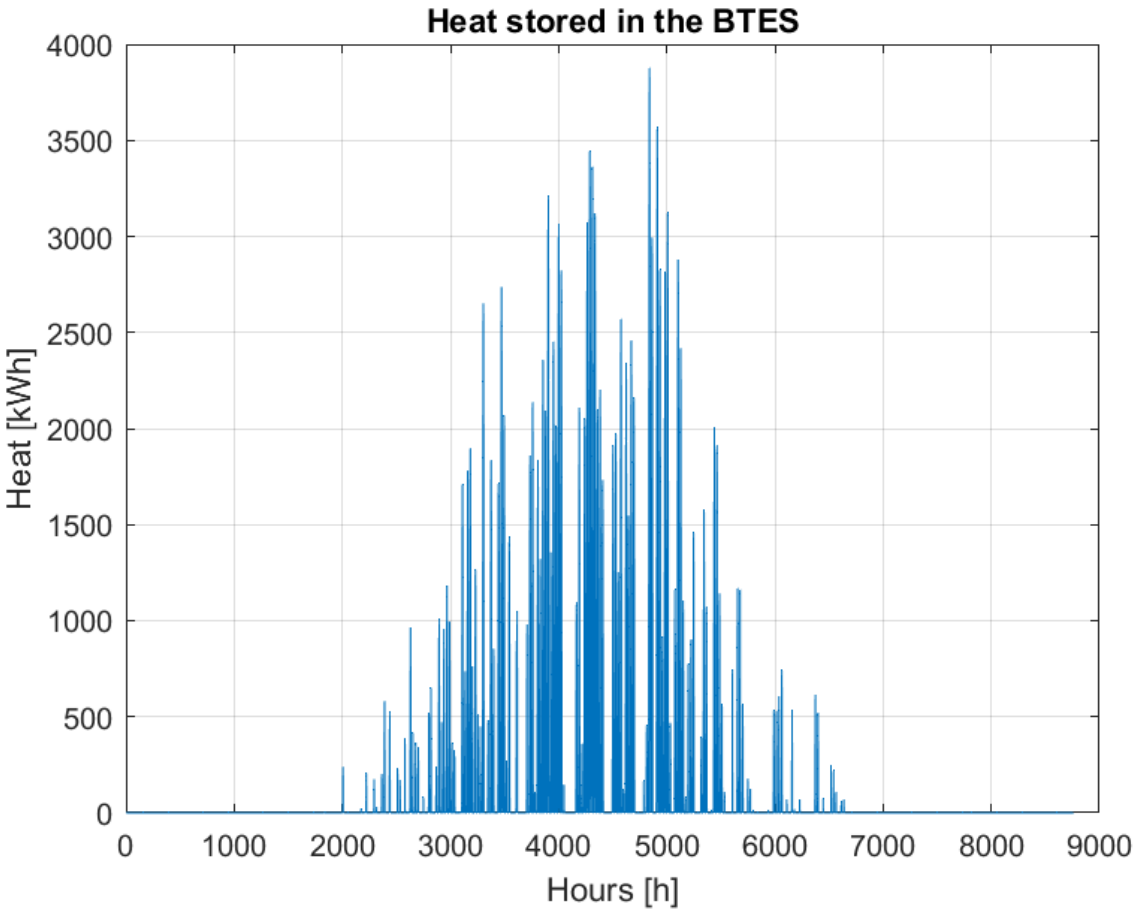

Figure 15: *Heat stored in the BTES during the year*

Figure 15 shows the total amount of heat stored in the BTES throughout the year. As the heat injected in the BTES is zero or close to zero for the first and last two thousand hours, as seen in figure 14, the amount of heat stored is zero in this period. In the summer months, the stored heat is fluctuating a lot, from zero to as much as almost 4000 kWh. This is in close coherence with figure 14, where there are large variations in injection and extraction of heat.

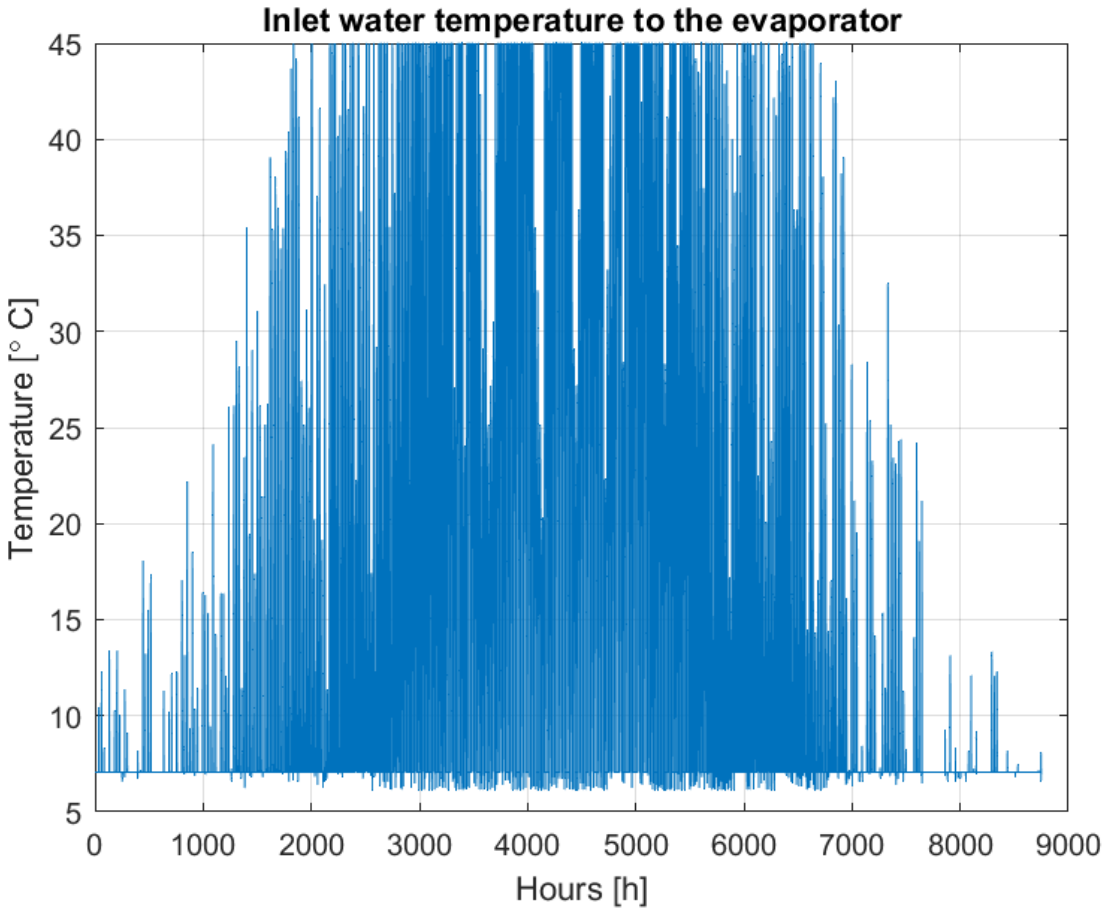

Figure 16: *Evaporator water/ethanol mixture inlet temperature*

In figure 16, the temperature of the water/ethanol mixture entering the evaporator is displayed, over the course of the year. There is a variation of almost 40 $°C$, where the maximum inlet temperature is 45 $°C$, and the minimum temperature is around 6 $°C$. During the winter months, the PVT system and BTES system is unable to heat the water/ethanol mixture to 45 $°C$ which is the desired temperature, as explained in section 3.7.1. During the summer, the temperature reaches 45 $°C$ at several instances, but also drops to the low temperatures around 6-7 $°C$.

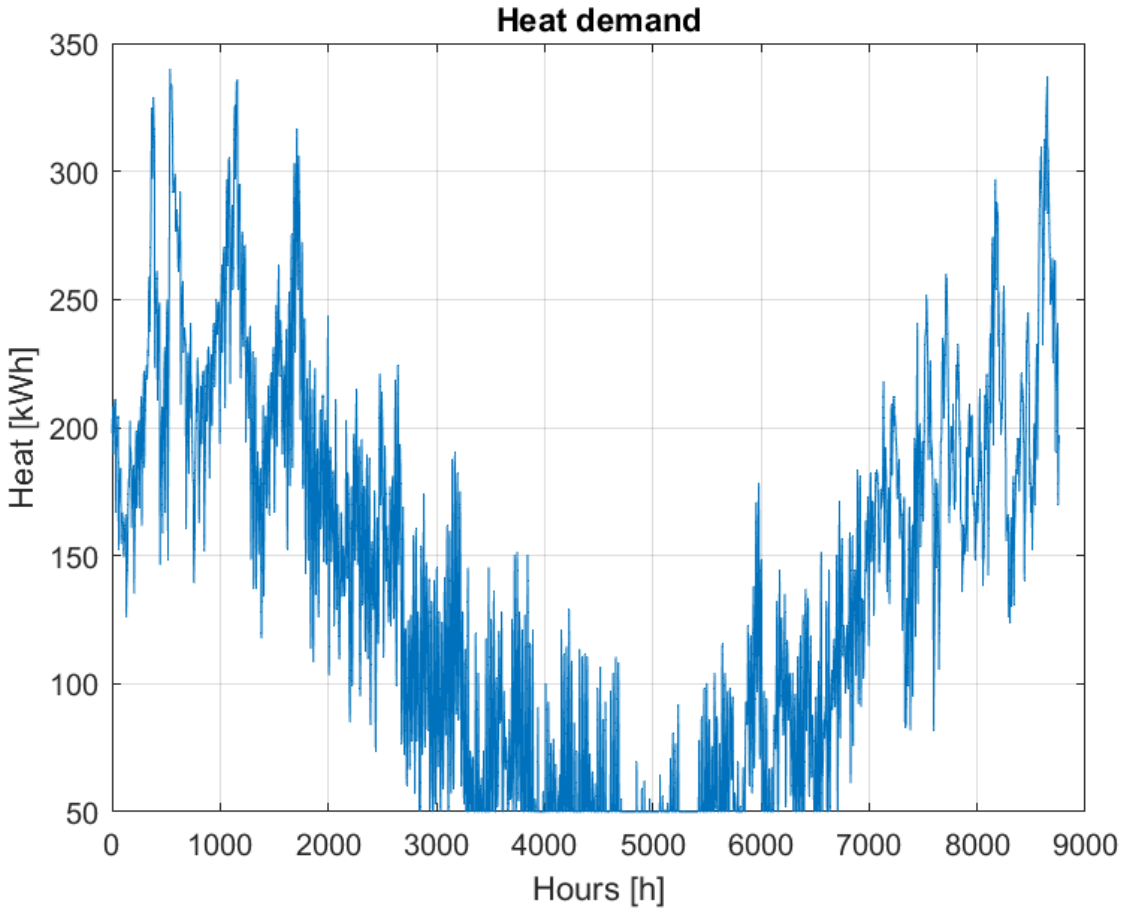

Figure 17: *Heat Demand during the entire year*

Figure 17 shows the heat demand throughout the entire year. There are large variations from winter to summer. During the winter, the demand is almost reaching 350 KWh at several hours, while for a period during the summer, the heat demand does not exceed 100 kWh. Even though there are large variations from season to season it is also large variations during a single season. During the first 1000 hours, the heat demand is as high as 340 kWh, but also as low as 125 kWh, which is a difference of 215 kWh.

	Number of hours [h]	Percentage of time [%]
Zero solar irradiance	4222	48.2
Empty BTES	7640	87.2
Excess heat from PVT system	845	9.6
Sufficient amount of heat from PVT and BTES system	1040	11.9

Table 3: *Overview of performance of the PVT and BTES system*

Table 3 show that the solar irradiance is zero 48.2 % of time during the year, which is almost half of the year. During these hours the heat and electric energy produced by the PVT system is zero as well. The BTES is empty most of the time during the year, which is also seen in figure 15, but better displayed in table 3. The PVT system is producing more heat than necessary only 9.6 % of the time during the entire year. This means in these hours, the BTES is charged. for approximately 12 % of the time, the PVT system produces enough heat to heat the water/ethanol mixture to 45 $°C$. This means that in 88 % of the time during the year, the PVT and BTES system is unable to produce the desired amount of heat.

4.1.2 January

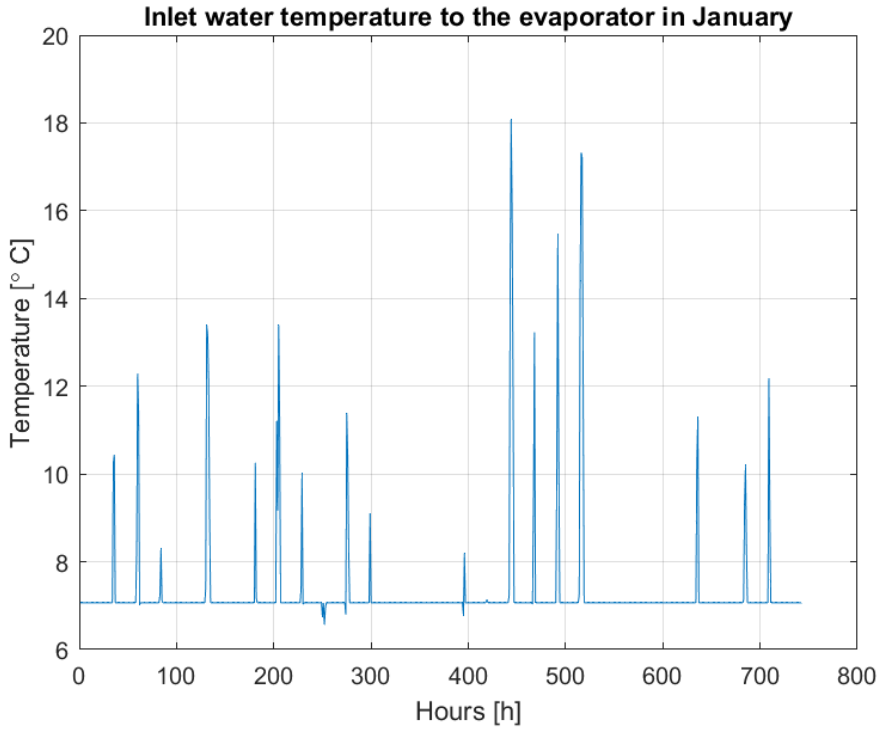

Figure 18: *Water/ethanol mixture temperature entering the evaporator in January*

Figure 18 shows the temperature of the water/ethanol mixture entering the evaporator in January. It is easier to interpret this figure compared to figure 16. The temperature is fairly consistent at at around 7 $°C$, with several tops in short intervals. The highest top reaches up to 18 $°C$, while most of the tops are around 12 $°C$. This is quite a large difference from the maximum temperatures reached in the summer as seen in figure 16.

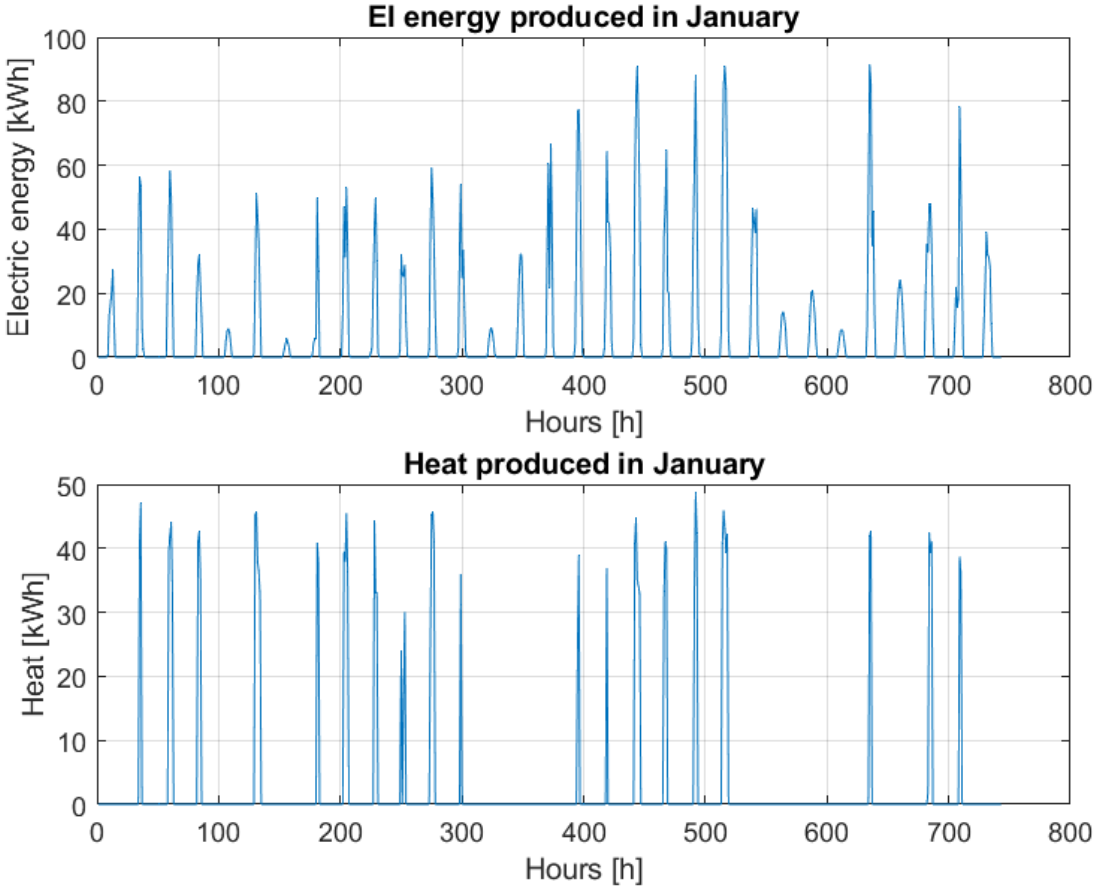

Figure 19: *Electric energy and heat produced by the PVT system in January*

Figure 19 shows the electric energy and heat produced by the PVT system in January. This is presented in order to easily interpret the results compared to the yearly results, just as mentioned in the paragraph above. It is seen that both the heat and electric energy production is drastically reduced compared to the summer months in figure 13 and 14. The heat production obtain tops around 40 kWh, but is most of the time zero during January. The electric energy production has more fluctuations than the heat production, and is reaching up to around 90 kWh, during January.

4.2 Summer

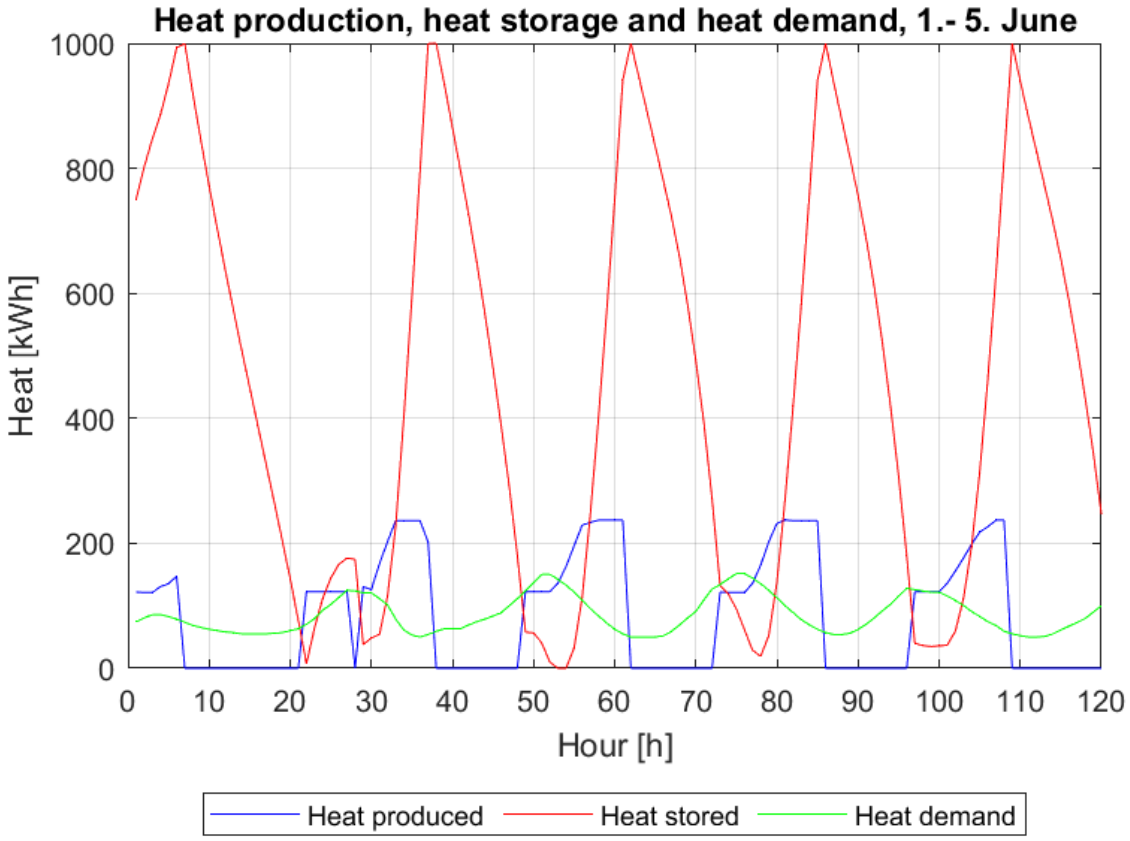

Figure 20: *Heat consumed, produced and stored*

20 shows the heat produced by the heat pump represented by the blue line, the heat stored in the TES represented by the red line, and the heat demand represented by the green line, over a five day period in June. This clearly shows that the heat pump is able to cover the heat demand from the district heating system as well as obtaining excess heat that can be stored in the TES. There is a clear cyclic behaviour of the heat pump production and the amount of heat that is stored. When the heat produced bu the heat pump is nonzero, the amount of heat stored is increasing, and when this amount reach its peak at 1000 kWh, the heat pump is shut off and the TES is discharged in order to cover the demand.

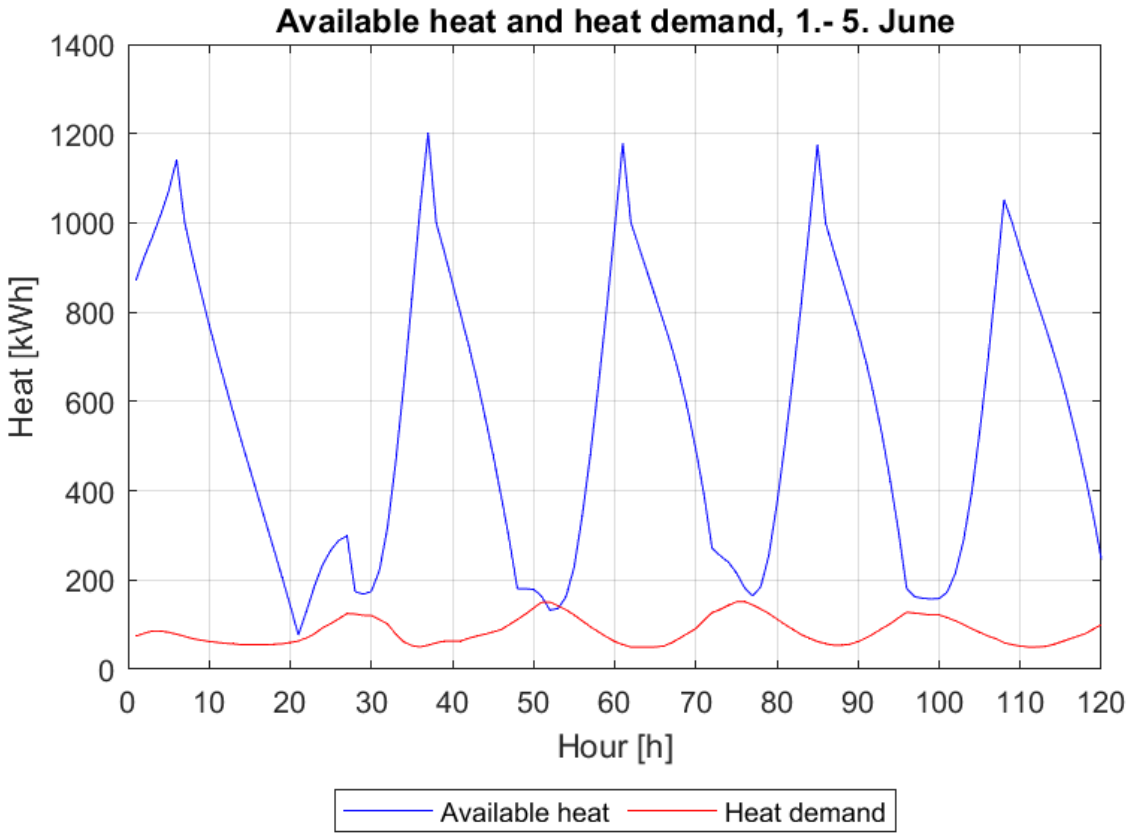

Figure 21: *Available heat and heat demand*

Figure 21 shows the available heat and heat demand, represented by the blue and red line respectively over a five day period in June. The available heat is the sum of the heat stored in the TES and the heat produced by the heat pump. The main objective of the heat pump is to always obtain more available heat than the heat demand, so the demand is always met. This is true for most of this period, but in time step 53 and 54, which is equivalent to hour number 3725 and 3726 in the year, the heat demand is not met. The demand exceed the available heat from the TES and heat pump which makes the heat pump insufficient to meet the required available heat. On the other hand, for most of the time during this period, the available heat is more than enough to cover the demand.

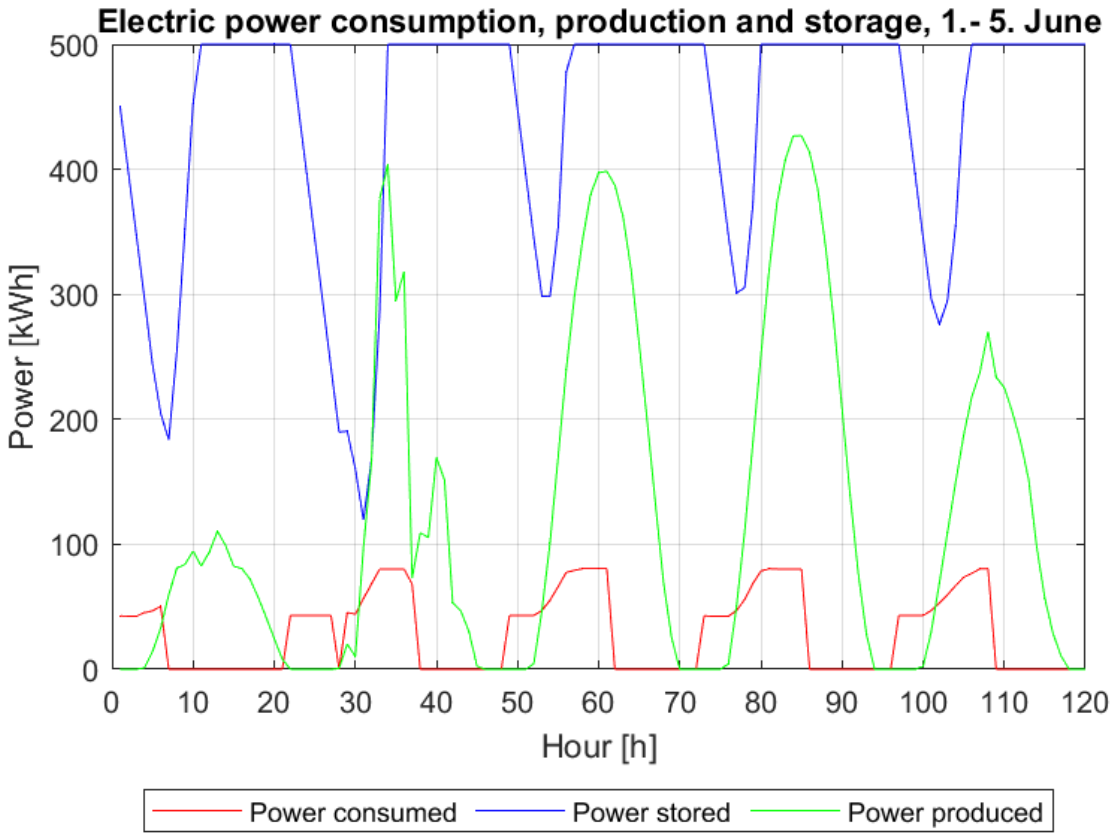

Figure 22: *Power consumed, produced and stored*

Figure 22 shows the electric power consumed by the compressor, produced by the PVT system and stored in the battery for a five day period in June, represented by the red, green and blue line, respectively. Just as in figure 20, there is a cyclic behaviour of the electric power curves. The amount of power stored in the battery is clearly decreasing whenever the power production from the PVT system is zero, and is increasing when the production exceeds the power demand from the compressors. The power demand never exceeds the amount of power stored for this period, which shows that the heat pump does not run on part load during this period.

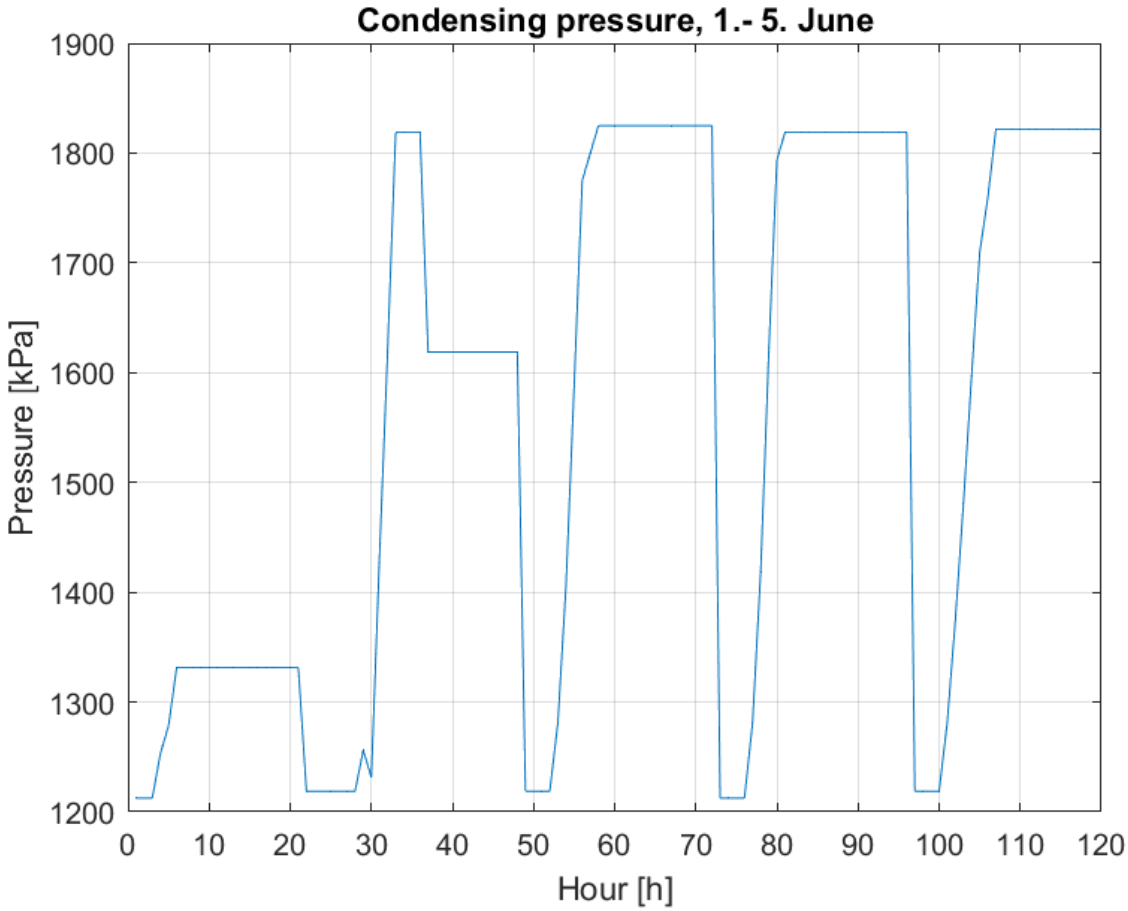

Figure 23: *Condensing pressure*

Figure 23 shows the pressure of the refrigerant during the condensation of a five day period in June. There are large fluctuations in the pressure and also the same cyclic behaviour as seen in the other figures in this result section. The pressure is down at 1218 kPa at the lowest points and reach up to 1825 kPa at the highest points. This means that the pressure fluctuate with more than 600 kPa and exceed the pressure used to dimension the components of 1800 kPa.

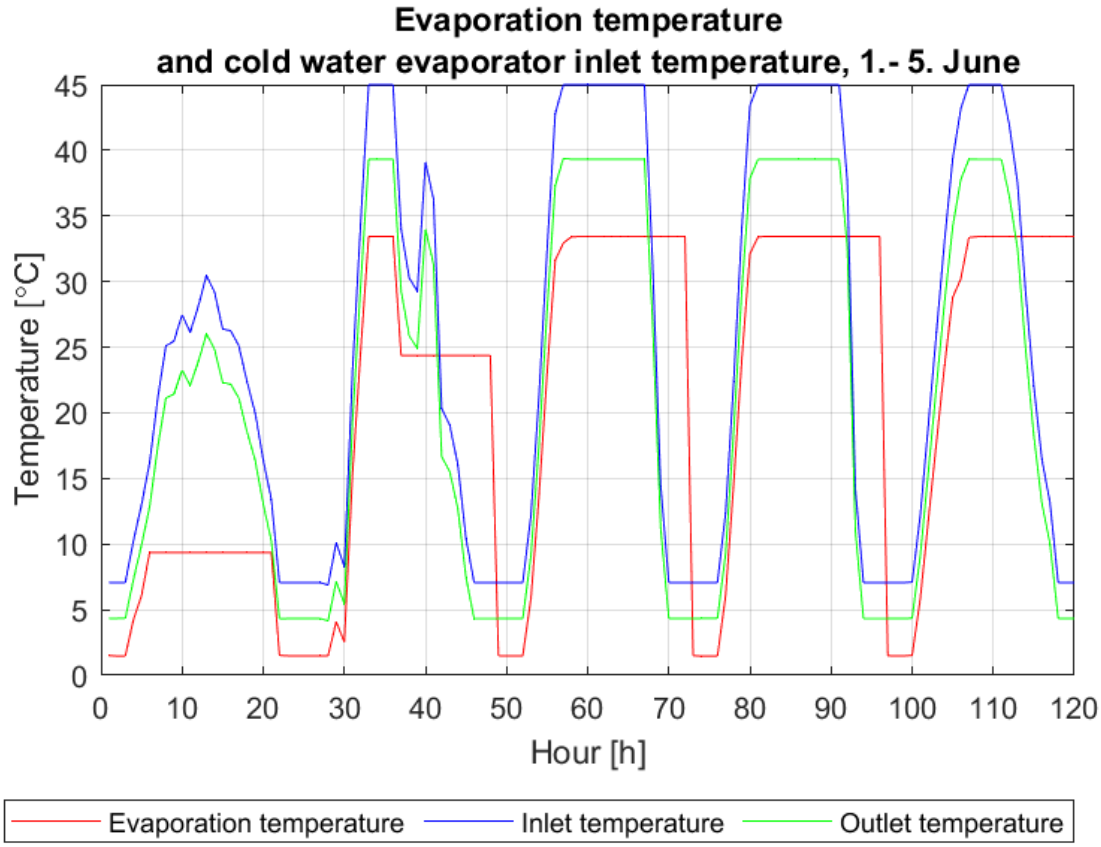

Figure 24: *Evaporation temperature, and evaporator inlet and outlet temperatures, 1. - 5. June*

Figure 24 shows the evaporation temperature of the refrigerant, along with the evaporator inlet and outlet temperature of the water/ethanol mixture, represented by red, blue and green line, respectively. The three temperature curves follow the same cyclic pattern. The inlet temperature exceed the outlet temperature which again exceed the evaporation temperature for most of the time. At the time steps around 45, 70, 95 and 115, the evaporation temperature is exceeding the other two temperatures. The trend is that the water/ethanol mixture temperatures drop, and then the evaporation temperature drops some hours after. Except this observation, the temperatures follow the same pattern.

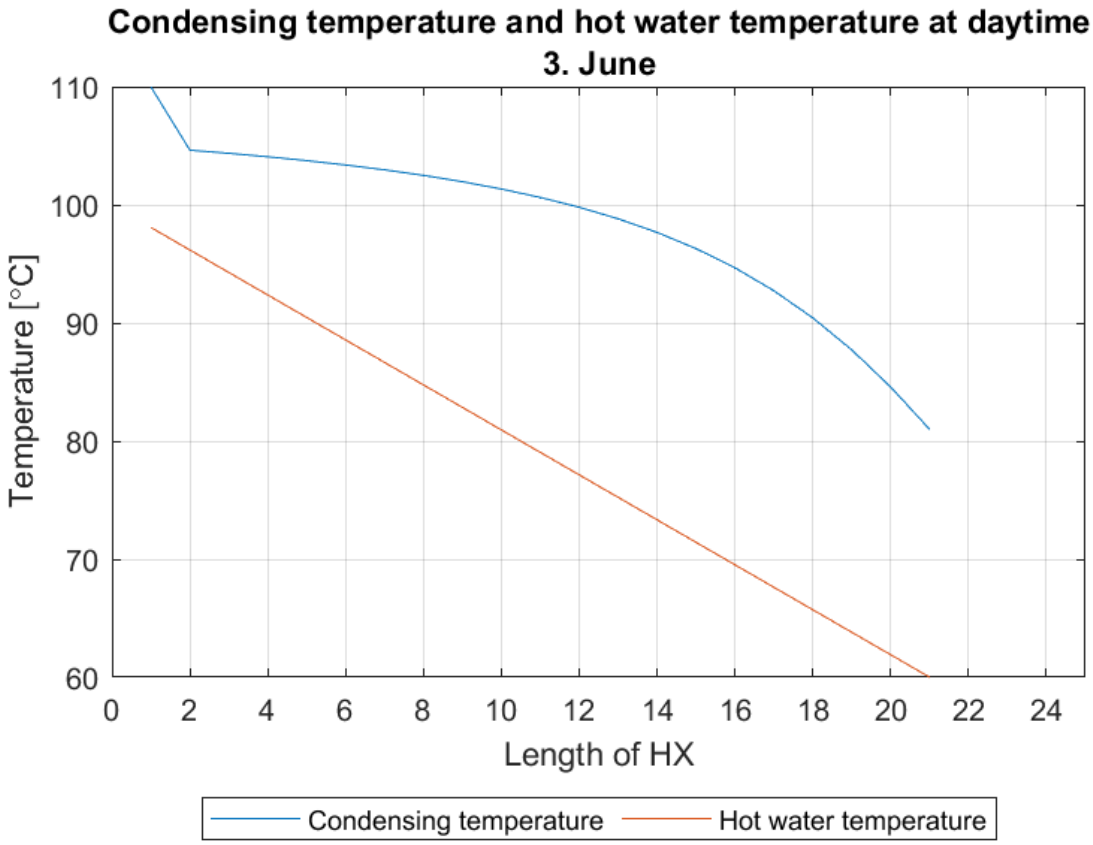

Figure 25: *Condensing temperature glide at daytime, 3.June*

Figure 25 shows the refrigerant temperature in the condenser and the water to be heated by the heat pump in the condenser, at daytime at the 3rd of June. The x-axis is not defined with a unit, because the temperature is calculated in 20 separate points as described in section **??**. The figure illustrates how the temperatures changes during the condensation and it is not of importance how this relates to the length of the heat exchanger. The water is coming in at 60 $°C$ and is heated to almost 100 $°C$ by the heat pump. The refrigerant is coming from the compressor at a temperature of 110 $°C$ and is cooled a bit before the the condensation process starts. The refrigerant outlet temperature is about 20 $°C$ larger than the water inlet temperature.

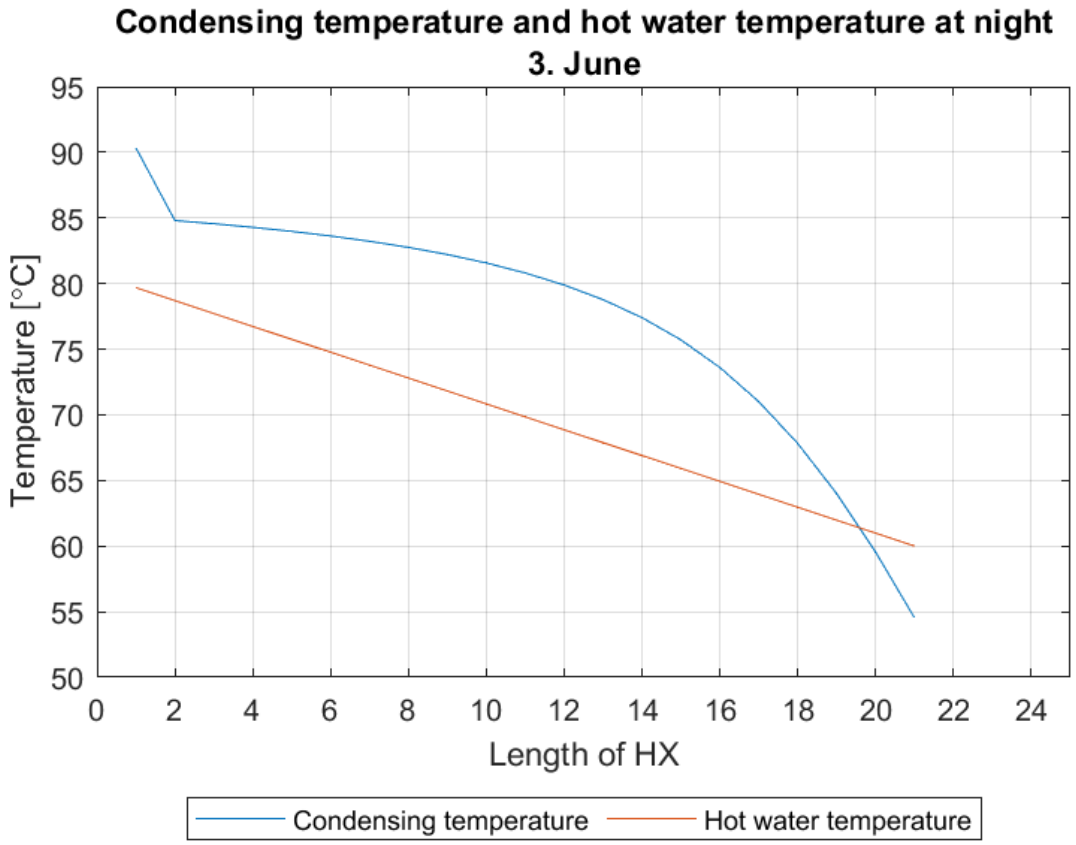

Figure 26: *Condensing temperature glide at night, 3.June*

Figure 26 is showing the same temperature curves as in figure 25, but at nighttime instead of daytime. In this figure the water is coming in at 60 $°C$, as this is set to be constant during the year in the code. The water is only heated to about 80 $°C$, instead of about 100 $°C$ which is desirable. This particular hour is the equivalent to hour number 51 in figure 20, where the heat demand exceeds the heat production from the heat pump. The pressure at this hour is also seen from figure 23 is equivalent to the low point of 1218 kPa. This result in a lower refrigerant inlet temperature of about 90 $°C$, and a refrigerant outlet temperature of about 55 $°C$. This is actually lower than the inlet water temperature, which tends to malfunctions in the code. It is also worth noticing that the temperature gradient of the refrigerant curve is steeper at the outlet compared to the curve in figure 25.

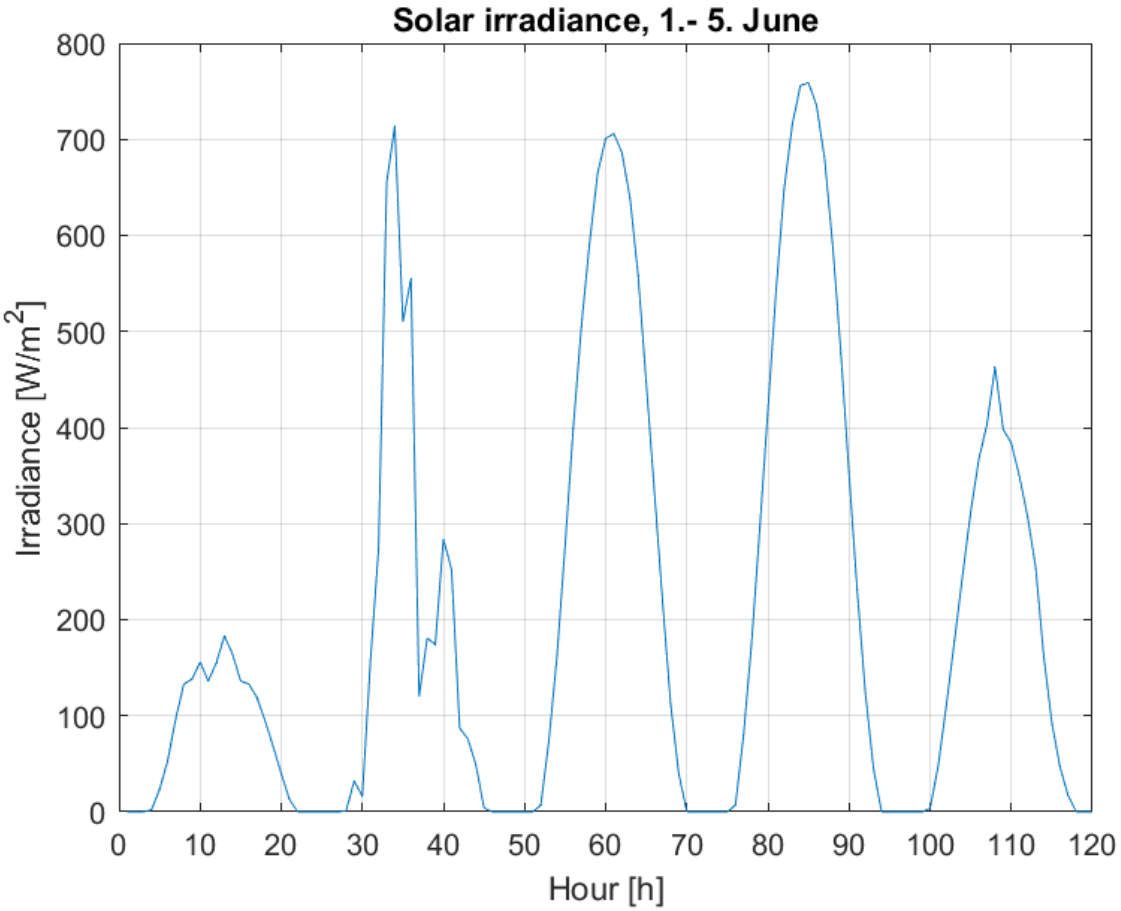

Figure 27: *Solar irradiance*

Figure 27 shows the solar irradiance for the five day period in June. The figure shows that there is more cloudy weather at the 1st and 5th of June, resulting in less solar irradiance, compared to the other days. Especially for the 1st of June, the solar irradiance is just below 200 $\frac{W}{m^2}$, which is almost $\frac{1}{4}$ of case for the 4th of June, where the solar irradiance almost reach 800 $\frac{W}{m^2}$.

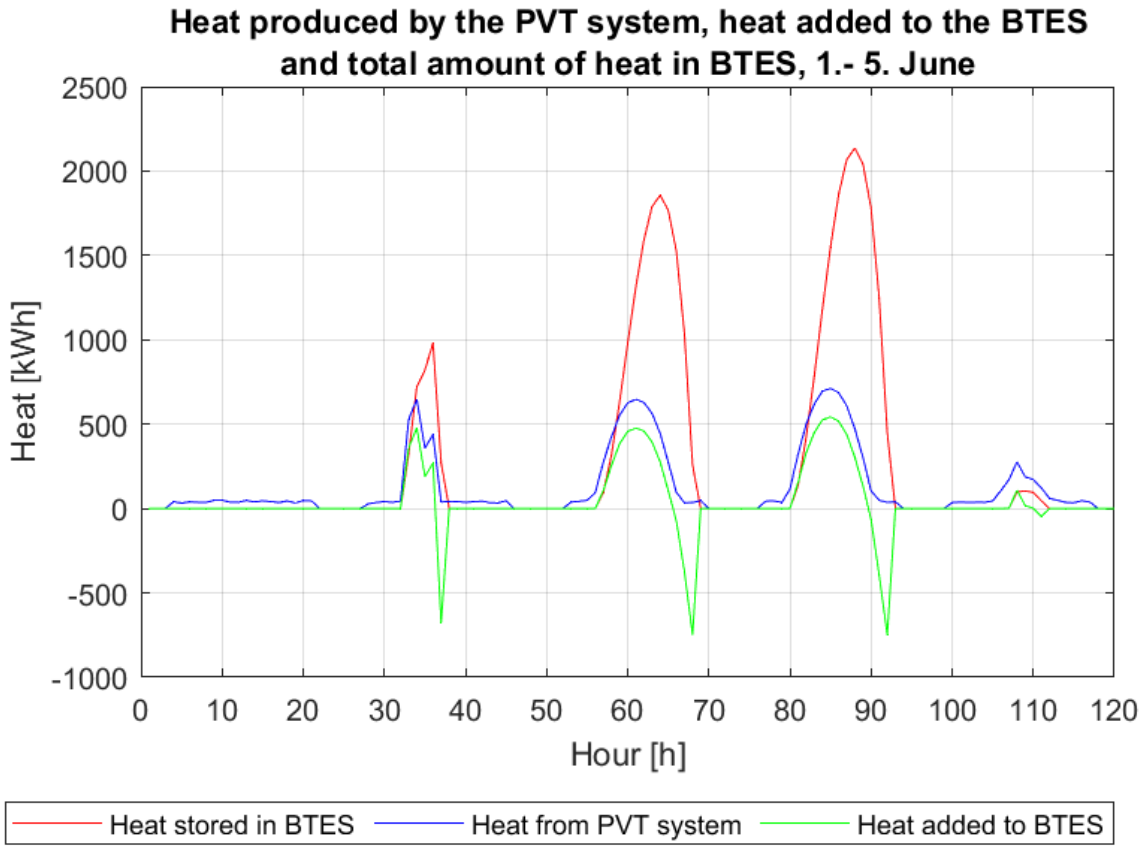

Figure 28: *Heat produced by the PVT system, heat added to the BTES, and total amount of heat stored in the BTES*

Figure 28 shows the heat produced by the PVT system, the heat inserted into the BTES, and the total amount of heat stored in the BTES, represented by the blue, red and green line, respectively. As seen in the figure, the PVT system produce very small amounts of heat at 1st and 5th of June compared to especially 3rd and 4th of June. The heat produced by the PVT system is slightly exceeding the curve representing the amount of heat directed to the BTES. This shows that the a part of the heat from the PVT system is directed to the BTES and the remaining heat is going to heat the water/ethanol mixture before the evaporator inlet. As the heat inserted to the BTES is positive, the total amount of heat stored is increasing, and starts to decrease when the heat is extracted from the BTES, which is shown when the green curve is below zero. When all of the curves are at zero, there is no production of heat from the PVT system or any heat stored in the BTES.

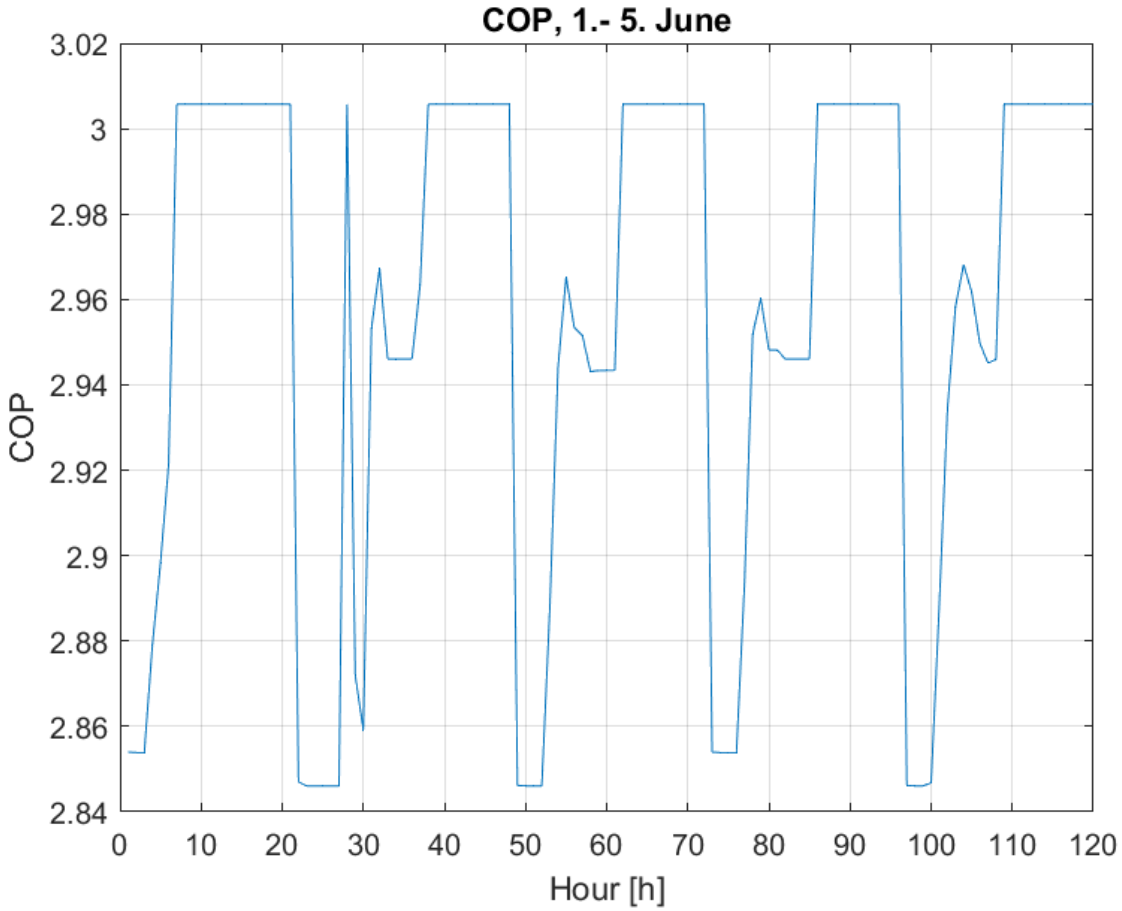

Figure 29: *COP*

Figure 29 shows the COP of the system during the five day period in June. The fluctuations in the COP are quite small, with only a 0.16 difference between the largest an smallest value. This shows that the COP is fairly consistent during this period.

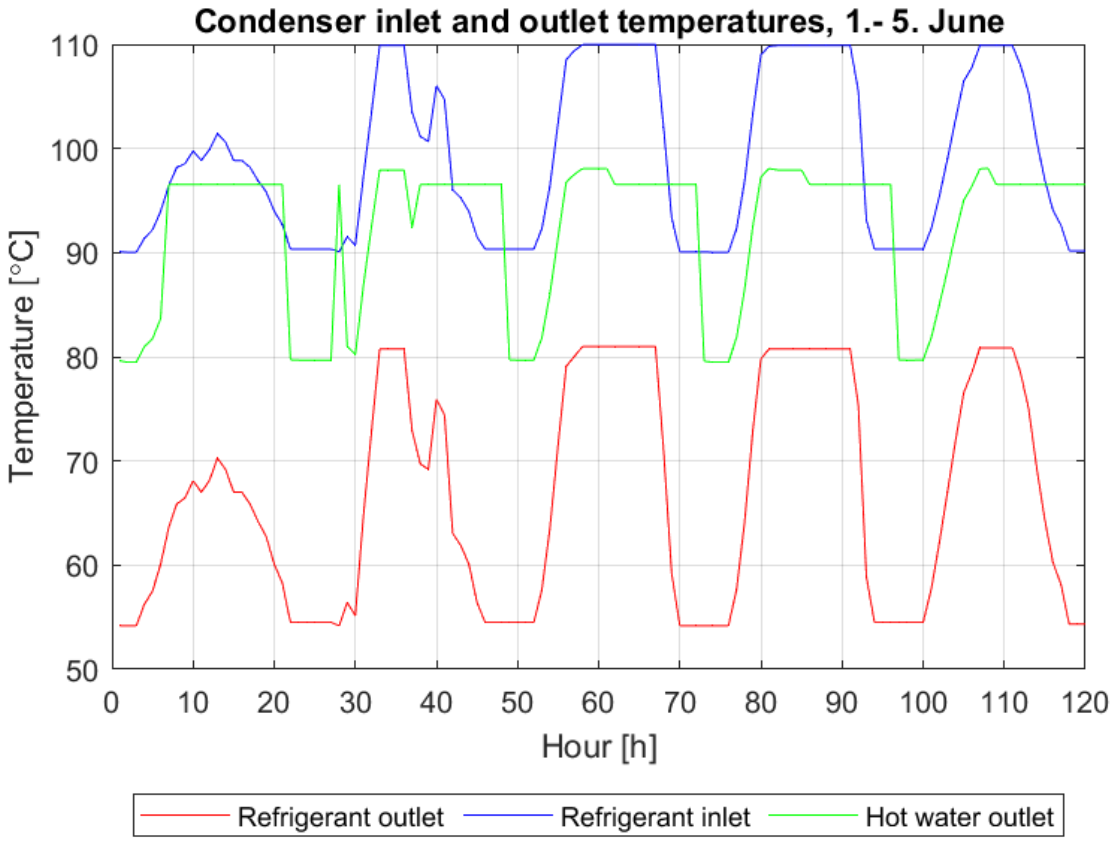

Figure 30: *Refrigerant inlet and outlet temperature of condenser, and hot water temperature out of condenser*

Figure 30 shows the refrigerant outlet and inlet temperatures of the condenser, and the hot water outlet temperature of the condenser, represented by the red, blue and green line respectively. The refrigerant outlet temperature is varying from approximately 55 $°C$ to 80 $°C$, which shows that the temperature is below the hot water inlet temperature, which is 60 $°C$, at several occasions. Additionally the hot water outlet temperature also seem to exceed the refrigerant inlet temperature at some instances. Just as for the evaporation temperature in figure 24, the hot water outlet temperature drops some hours later than the other two temperature curves. Apart from that, the temperatures follow the same fluctuations, where the hot water outlet temperature is mostly between the refrigerant inlet and outlet temperature.

5 Discussion

5.1 Energy system performance

Because of the malfunctions addressed in the introduction in section 4, the results regarding the heat pump performance were limited to a short period in June, representing the summer. However, the performance during other time periods of the year will be discussed based on the other parts of the energy system, that were presented in 4.1.1. The performance of the heat pump during the summer will be discussed, and how the other parts of the energy system affect the heat pump.

During the summer, the heat demand is at it lowest during the year, and at the same time, the heat and electricity production is at it highest. Because of this it is clear that the heat pump along with the TES is able to cover the demand in almost all of the hours during the five day period in June. However, for a small period of the five days, the demand is not met. This happens during the night hours as the heat demand curve is at one of its tops due to low outside temperatures. In these two hours, the ambient temperature is 5.2 $°C$ and 6 $°C$. The TES is only empty in hour number 54 and 55 during the whole five day period, showing that during that night the TES was emptied faster compared to the other nights. This resulted in a case were the heat pump needed to cover the demand alone, and was unable to.

As for the electric power demand, consumption and storage curves showed in figure 22, the power demanded by the compressors are covered with a large margin during the five days. Despite this, the heat pump is unable to produce enough heat to cover the demand for two hours. The solar irradiance tops in figure 27 are one of the highest during the entire year, resulting in large electric energy production, which is then successfully stored in the battery when necessary. The battery is at maximum capacity for 65 % of the time during the five days, showing that there is produced a lot of excess electric energy during the summer months.

The electric energy production is sufficient during the five days, and at the same time the maximum demand during the five days is only 44 % of the maximum demand of the entire year. Still, the energy system is unable to cover the demand for the entire five day period. Based on this, it is likely that the energy system is unable to cover the demand in many more time steps during the other seasons, especially winter. When the demand approaches 340 kWh during the coldest days, and the same time the electric energy production makes the heat pump run on part load it is clear that the energy system fails to operate as desired.

For the first half of January, the PVT system is unable to produce more than 60 kWh of electric energy as seen in figure 19. As seen in figure 22, the power consumed by the compressor reaches up to 80 kWh for several time steps during the five day period in June. Based on this it seems that heat pump must operate on part load over larger periods during the winter. Additionally, the ratio of the maximum heat produced in a single hour in January and in July is only 4.6 %. This is reflected in figure 18, where the peak temperature is only 18 $°C$ in January, due to the PVT systems inability to produce enough heat.

Based on the solar irradiance curve in figure 13, it is likely that the results presented in section 4.2 is representative for the entire summer. That is, in most of the hours during the summer, the heat pump and TES is able to cover the heat demand. However, When the available heat is at its lowest during the nights in figure 21, the available heat curve only exceed the heat demand by a small margin. Therefore it is likely that the available heat is insufficient in several instances during the summer. Based on the results in section 4.2 alone, a larger TES could be a solution. There are several cases during the five days in June, where the TES capacity reaches its maximum, and the heat pump is shut off even when it could produce more heat. The heat pump is shut off 51.2 % of the time during the five days in June, even though there is sufficient amount of electric power to run the compressor the entire period. By increasing the capacity of the TES, the potential of the heat pump could be utilized better by producing more heat and storing it.

Even though a larger TES capacity would solve some problems during the summer operation, it is likely that for the energy system to operate ideally during the entire year, more changes needs to be done. The ratio of the maximum solar irradiance in a single hour in January and in the five day period in June is 19 %. From figure 15 and table 3, it is clear that the BTES and PVT system is not operating as desired. During the winter, it is desirable to have heat stored in the BTES that can be utilized when the heat production from the PVT system is low. This is not the case, as the BTES is empty for as much as 87.2 % of the time during the entire year. In fact, the BTES is empty for all of January, February, November and December. During these months the heat pump capacity will be drastically reduced compared to the summer operation, due to lack of electric power and low heat source temperatures. It is therefore likely that the heat produced by the heat pump during these months will go directly to cover the heat demand. A larger TES capacity will not improve the performance of the energy system during these months because the TES will not reach its maximum.

In order to improve the overall energy system, the main focus should be on how to increase the heat source temperatures. Since the BTES is so far away from working as desired, this should be the component that is optimized first in the energy system. Solar power is in general a poor energy source to utilize in Oslo, Norway. As mentioned in section 2.4, the solar radiation in Oslo is quite low compared to several Asian countries, and areas around the equator. Although, a possible option is to increase the area of the PVT panels, in order to produce more heat. This will likely reduce the issue with low heat source temperatures but it will probably not eliminate it entirely. It seems like the heat production from the PVT system is so low that in order to obtain an evaporator inlet temperature of 45 $^{\circ}C$ the area of the PVT panels would need to be excessively large.

A possible option is to use a second heat source in order to increase the temperature of the water/ethanol mixture entering the evaporator. A heat source that is not affected by the ambient conditions as much as solar power would be desirable. Waste heat from industrial processes often hold relatively high temperatures, and is also used in many HTHP applications today as mentioned in section 2.2. By including this as a heat source the energy system could enhance its performance compared to its current state.

The BTES is currently working as a short term storage system, where it is charged and charges/discharged on an hourly basis. As mentioned it is only during the summer, that the BTES is charged due to lack of heat production during the other seasons. The BTES is therefore discharged and emptied during the nighttime in the summer, when the heat production from PVT system is at zero. If a larger area of the PVT panels is applied and a second heat source, resulting in larger heat production the BTES system could be alternated. A TES system similar to the one used in the district heating line could be used to cover the short term storage when the heat from the PVT is low at nighttime. Additionally, a larger BTES systen could be used for seasonal storage when there is larger periods with low heat production from the PVT system.

In January the total heat demand was 162.9 MWh. If the heat pump was able to produce 250 kW without shutting off throughout January it would produce 186 MWh. That means that the heat pump could produce more heat than the heat demand in total. However, in order to do this, it is necessary with sufficient electric power to run the compressors and high enough heat source temperatures. Additionally, since the heat demand reaches almost 350 kWh in certain hours, the heat pump would be dependant on the TES supplying with heat in those instances. However, it seems unlikely that the heat pump is able to cover the demand and also acquire excess heat to charge up the TES. Therefore it seems like a larger capacity of the heat pump is required, in addition to a larger TES capacity, larger area of PVT panels and also an additional heat source.

A larger area of the PVT panels will result in more electric energy production as well as heat production. As mentioned, it seems like during the summer, the electric power demand is covered by the PVT system and battery. In January, however, the total electric power demand will be higher because the heat pump must run more often. The power production from the PVT system will at the same be lower. If the compressors demanded 80 kWh every hour throughout January, it would be demanded 59.52 MWh, while the electric energy production from the PVT system in January is 5.26 MWh. It is therefore optimal to have larger heat capacity and TES capacity so the heat pump can be shut off, and the power demand will be reduced. It seems like a larger battery capacity also could be beneficial due to the large difference between production and demand.

The evaluation of the COP, which is one of the most used parameters to evaluate the performance of a heat pump, is heavily affected by the fact that the code is unable to run the entire year. The COP displayed in figure 29 shows relatively low COP values. When the heat pump is shut off, the COP is set to a value of 3.005, which is the COP obtained when the script used to dimension the heat pump is ran. Therefore the COP is kept constant at 3.005 for several hours, before dropping. It is clear that the heat pump is performing poorer than desired and expected. There are clearly some malfunctions in the code, which is addressed already, and this could affect the COP. The poor COP could also be affected by poor optimizing of different parameters, such as the cascade temperatures, which is mentioned below in 5.2. Based on the COP presented in figure 29, however, it seems like the utilization of a temperature glide in the condenser did not affect the performance as desired.

5.2 Temperatures

The heat source temperature have been discussed some already, related to the overall performance of the energy system. However there are other aspects of the different temperatures that need to be addressed and discussed. In figure 24, as mentioned, the evaporation temperature seem to be a bit delayed compared to the inlet and outlet temperature of the water/ethanol mixture. When the water/ethanol mixture temperatures drop, the evaporation temperature is kept constant for a few hours before it also drops. This is due to the development of the code. In the code, when the heat pump is shut off, several parameters are set to be equal the the value obtained in the previous iteration, or hour. This includes the lmtd of the compressor, the evaporation temperature, the temperatures in the cascade heat exchanger and the pressure.

If figure 24 and figure 22 is compared, it is clear that the evaporation temperature exceeds the water/ethanol mixture temperatures only when the heat pump is shut off. Ideally, the evaporation temperature can not exceed the heat source temperature, because the refrigerant in the evaporator is supposed to be absorbing the heat from the water/ethanol mixture. However, when this happens only when the heat pump is off, it seems like this part of the code work as desired, and there is not any complications.

The same procedure happens with the condenser outlet water temperature and the condenser inlet refrigerant temperature. In the code the water temperature is set to 96.5 $°C$ when the heat pump is turned off. In figure 30, the water temperature exceeds the refrigerant inlet temperature at some instances, but this happens only when the heat pump is turned off. However, in the other end of the condenser, there are some complications. The water inlet temperature is constant at 60 $°C$ during the entire year. As seen in figure 30 this water temperature exceed the refrigerant outlet temperature at several instances, also when the heat pump is turned on. This shows that there are some parts of the code related to the calculation of the LMTD and heat capacity in the condenser, that is not working optimal.

The same problem can be seen in figure 26, where the temperature curves are plotted for the 3rd of June, at nighttime. In this case, it is seen from figure 28 that there is no available heat to heat the water/ethanol mixture. This results in an evaporation temperature of 1.48 $°C$, and a condensing pressure of 1218 kPa. The water temperature exiting the condenser and the refrigerant temperature entering the condenser are reduced with almost the same amount, but since the the inlet water temperature remains constant, the refrigerant outlet temperature is reduced too much. It is also clear that the temperature curve is steeper at lower pressures as figure 25 and 26 shows.

As mentioned in section 2.1, the temperature glide in a zeotropic mixture is induced by the difference between the boiling points of the components. Therefore normally a larger difference between the boiling points, result in larger temperature glide. For the case in figure 25, the condensing pressure is 1825 kPa, and the difference between the saturation temperatures of CO_2 and butane at this pressure is 131.8 $°C$. When the condensing pressure is 1218 kPa, the difference in saturation temperatures is 123.4 $°C$. That means that, even though the difference in the saturation temperature

of the two components are less for the case with a condensing pressure of 1825 kPa, the temperature glide is larger for the case with a condensing pressure of 1218 kPa.

The temperatures in the cascade heat exchanger is not optimized as much as it could be. Like in the paper by Zou et al. (2020), which was discussed in section 1.2.1, an optimization algorithm could be applied in order to optimize the temperatures in the cascade heat exchanger. In the current code the temperatures in the cascade heat exchanger are just a simple calculation based on the condenser temperature glide and the evaporation temperature. It is very likely that an optimization of the pressure ratio in each cycle could affect the overall performance of the heat pump in a positive manner.

6 Conclusion and further work

In this thesis a high temperature heat pump have been simulated together with a battery, a PVT system, a TES system using a PCM. These components constitutes an integrated energy system that is supposed to deliver heat to a district heating system. The components are simulated in Matlab, and in the thesis an evaluation on how the heat pump worked in coherence with the other components was conducted. The energy system was simulated for every hour throughout an entire year, based on weather data collected from Oslo, Norway in 2005.

Some problems regarding the software was a recurring incident during the work with this thesis. Matlab encountered internal problems often when the code was running, forcing the software to close. This happened often at different times during the simulation, which manifested that there was not any specific error in the code leading to the internal problems. The many loops and iteration, combined with the calculations could be the issue, but it was never confirmed why this happened. Nevertheless, some results were constructed, and interpreted. The entire energy system was simulated for five days in June, while the BTES and PVT system was simulated for the entire year. Based on these simulations, the performance of the overall energy system throughout the entire year was evaluated.

Since the energy system was unable to cover the heat demand throughout the entire five day period in June, the performance of the system is clearly poor. During the five day period in June, the maximum solar irradiance is 5.2 times larger than the maximum solar irradiance in January. When the heat demand is unable to be fulfilled during a few hours in June, it is likely that the heat demand is uncovered during relatively large periods in the winter. In the winter, the demand is higher, and the heat and electric energy production is lower compared to the summer. Therefore, it is clear that the integrated energy system does not function as desired.

A larger area of the PVT panels to produce more heat and electric energy is a viable option, in order to enhance the performance of the energy system. A second heat source could also increase the heat source temperatures during the winter, which in turn would enhance the performance of the overall system. A larger capacity of the TES and heat pump are also options that could be

considered to improve the system.

The COP of the heat pump is relatively low during the five day period in June. The COP is fluctuating between 2.85 to 3 which is far from the desired value of 3.6. This could be caused by malfunctions in the code. Nevertheless, the choice of refrigerants and configuration does not seem to be appropriate choices due to the low COP. Optimization algorithms of different parameters, such as cascade heat exchanger temperatures could increase the COP and the heat pump performance.

The two fluid temperature curves in the condenser are crossing each other at several instances during the simulation in June. This is clearly not possible in a heat exchanger, which reveal that there are malfunctions in the code regarding the calculation of these temperatures. The process of calculating the condensing pressure seems to be the problem. This process is unable to converge when the heat pump is operating on part load.

In further work on this thesis, there are several aspects that need improvement. First of all, the code need to be updated so it is able to run throughout the entire year. The condensing pressure algorithm is probably the main part that needs improvement. Additionally, the BTES, PVT, battery, and TES systems contain a lot of simplifications. In the further work, more detailed models need to be created in order to obtain more realistic results. Additionally, the pressures in the two stages in the heat pump, and the temperatures in the cascade heat exchanger can be optimized in order to reach as high COP as possible.

References

5.7 Azeotropic/Zeotropic refrigerants - SWEP (n.d.).
URL: *https://www.swep.net/refrigerant-handbook/5.-refrigerants/sd1/*

AIKINS, K. A., LEE, S.-H. & CHOI, J. M. (2013), 'TECHNOLOGY REVIEW OF TWO-STAGE VAPOR COMPRESSION HEAT PUMP SYSTEM', *http://dx.doi.org/10.1142/S2010132513300024* **21**(03), 1330002.

Alva, G., Lin, Y. & Fang, G. (2018), 'An overview of thermal energy storage systems', *Energy* **144**, 341–378.

Arpagaus, C., Bless, F., Uhlmann, M., Schiffmann, J. & Bertsch, S. S. (2018), 'High temperature heat pumps: Market overview, state of the art, research status, refrigerants, and application potentials', *Energy* **152**, 985–1010.
URL: *https://doi.org/10.1016/j.energy.2018.03.166*

Banister, C. J. & Collins, M. R. (2015), 'Development and performance of a dual tank solar-assisted

heat pump system', *Applied Energy* **149**, 125–132.

Chamoun, M., Rulliere, R., Haberschill, P. & Peureux, J. L. (2014), 'Experimental and numerical investigations of a new high temperature heat pump for industrial heat recovery using water as refrigerant', *International Journal of Refrigeration* **44**, 177–188.

Dai, B., Dang, C., Li, M., Tian, H. & Ma, Y. (2015), 'Thermodynamic performance assessment of carbon dioxide blends with low-global warming potential (GWP) working fluids for a heat pump water heater', *International Journal of Refrigeration* **56**, 1–14.
URL: *www.sciencedirect.comhttp://dx.doi.org/10.1016/j.ijrefrig.2014.11.0090140-7007/*

Dincer, I. & Rosen, M. M. A. (2011), 'Thermal energy storage : systems and applications', p. 599.

Eikevik, T. M. (n.d.), 'Heat Pumping Processes and Systems'.
URL: *http://folk.ntnu.no/tme*

Engineering ToolBox (2020).
URL: *https://www.engineeringtoolbox.com/heat-transfer-coefficients-exchangers-d*$_4$50*.html*

Fernández-Moreno, A., Mota-Babiloni, A., Giménez-Prades, P. & Navarro-Esbrí, J. (2022), 'Optimal refrigerant mixture in single-stage high-temperature heat pumps based on a multiparameter evaluation', *Sustainable Energy Technologies and Assessments* **52**, 101989.

Greenhouse Gas Emissions from Energy Data Explorer – Analysis - IEA (n.d.).
URL: *https://www.iea.org/articles/greenhouse-gas-emissions-from-energy-data-explorer*

Guo, H., Gong, M. & Qin, X. (2019), 'Performance analysis of a modified subcritical zeotropic mixture recuperative high-temperature heat pump', *Applied Energy* **237**, 338–352.

He, Y., Cao, F., Jin, L., Wang, X. & Xing, Z. (2015), 'Experimental study on the performance of a vapor injection high temperature heat pump', *International Journal of Refrigeration* **60**, 1–8.

Heating – Analysis - IEA (n.d.).
URL: *https://www.iea.org/reports/heating*

Herrando, M., Ramos, A., Zabalza, I. & Markides, C. N. (2019), 'A comprehensive assessment of alternative absorber-exchanger designs for hybrid PVT-water collectors', *Applied Energy* **235**, 1583–

1602.

Jouhara, H., Żabnieńska-Góra, A., Khordehgah, N., Ahmad, D. & Lipinski, T. (2020), 'Latent thermal energy storage technologies and applications: A review', *International Journal of Thermofluids* **5-6**(6), 100039.
URL: *http://creativecommons.org/licenses/by/4.0/*

Kannan, N. & Vakeesan, D. (2016), 'Solar energy for future world: - A review', *Renewable and Sustainable Energy Reviews* **62**, 1092–1105.
URL: *http://dx.doi.org/10.1016/j.rser.2016.05.022*

Lamnatou, C. & Chemisana, D. (2017), 'Photovoltaic/thermal (PVT) systems: A review with emphasis on environmental issues', *Renewable Energy* **105**, 270–287.

Lazzarin, R. & Noro, M. (2020), 'Photovoltaic/Thermal (PV/T)/ground dual source heat pump: Optimum energy and economic sizing based on performance analysis', *Energy and Buildings* **211**, 109800.

López-Martín, R. & Valenzuela, L. (2018), 'Optical efficiency measurement of solar receiver tubes: A testbed and case studies', *Case Studies in Thermal Engineering* **12**, 414–422.

Maccallum, R. N., Fisher, K. S., Kenneth, P. E. & Mcintush, E. (n.d.), 'Flammability of Mixtures of CO 2 and Hydrocarbons'.
URL: *www.oxy.com*

Moran, M. J., Shapiro, H. N., Boettner, D. D. & Bailey, M. B. (2018), *Principles of engineering thermodynamics*, 9th edn, Wiley.

Mota-Babiloni, A., Mateu-Royo, C., Navarro-Esbrí, J., Molés, F., Amat-Albuixech, M. & Barragán-Cervera, (2018), 'Optimisation of high-temperature heat pump cascades with internal heat exchangers using refrigerants with low global warming potential', *Energy* **165**, 1248–1258.
URL: *https://doi.org/10.1016/j.energy.2018.09.188*

Panel Solar Híbrido ECOMESH - ENDEF (n.d.).
URL: *https://endef.com/panel-solar-hibrido/ecomesh/?lang=en*

Qu, M., Chen, J., Nie, L., Li, F., Yu, Q. & Wang, T. (2016), 'Experimental study on the operating characteristics of a novel photovoltaic/thermal integrated dual-source heat pump water heating

system', *Applied Thermal Engineering* **94**, 819–826.

Radermacher, R. & Hwang, Y. (2005), Vapor compression heat pumps with refrigerants mixtures, 1 edn, CRC Press, pp. 17–22.

Ryssdal, S. T. (2020), High Temperature Heat Pumps in Integrated Energy Systems, Technical report.

Sarkar, J. & Bhattacharyya, S. (2009), 'Assessment of blends of CO2 with butane and isobutane as working fluids for heat pump applications', *International Journal of Thermal Sciences* **48**(7), 1460–1465.
URL: *https://linkinghub.elsevier.com/retrieve/pii/S1290072908002846*

Singh, G. K. (2013), 'Solar power generation by PV (photovoltaic) technology: A review', *Energy* **53**, 1–13.
URL: *http://dx.doi.org/10.1016/j.energy.2013.02.057*

Yao, J., Liu, W., Zhang, L., Tian, B., Dai, Y. & Huang, M. (2020), 'Performance analysis of a residential heating system using borehole heat exchanger coupled with solar assisted PV/T heat pump', *Renewable Energy* **160**, 160–175.

Yu, X., Zhang, Y., Deng, N., Chen, C., Ma, L., Dong, L. & Zhang, Y. (2014), 'Experimental performance of high temperature heat pump with near-azeotropic refrigerant mixture', *Energy and Buildings* **78**, 43–49.

Zou, H., Li, X., Tang, M., Wu, J., Tian, C., Butrymowicz, D., Ma, Y. & Wang, J. (2020), 'Temperature stage matching and experimental investigation of high-temperature cascade heat pump with vapor injection', *Energy* **212**, 118734.

Zuev, O. A., Garanov, S. A., Ivanova, E. V. & Karpukhin, A. S. (2020), 'Investigation of the Efficiency of Autocascade and Cascade Heat Pumps in Cold Climate', *Chemical and Petroleum Engineering* **56**(5-6), 448–455.

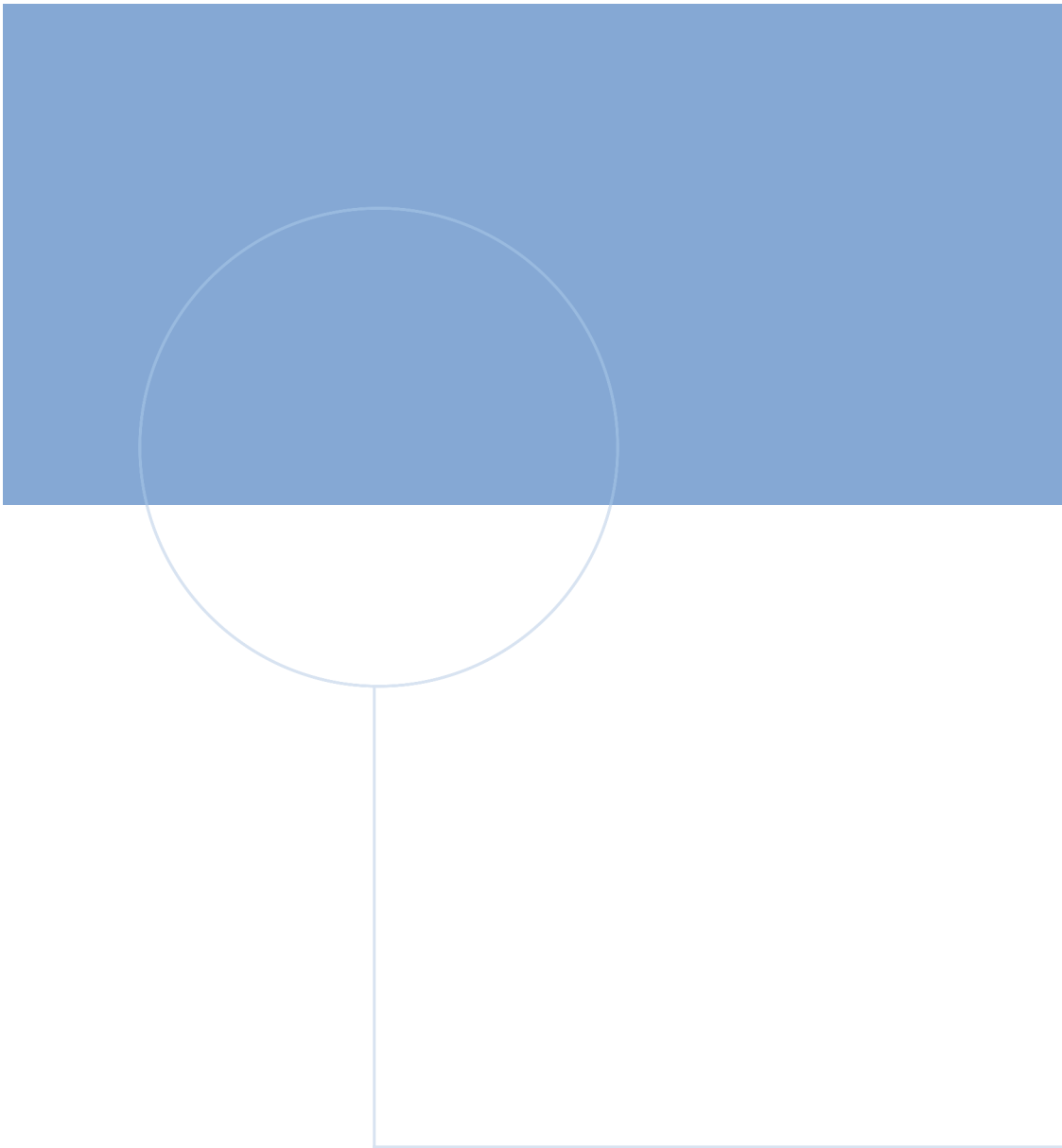

NTNU

Kunnskap for en bedre verden